PERFORMANCE ANALYSIS OF GROOVED HEAT PIPES USING 3-D MULTI-CHANNEL THERMAL RESISTANCE NETWORK

A THESIS SUBMITTED TO
THE GRADUATE SCHOOL OF NATURAL AND APPLIED SCIENCES
OF
MIDDLE EAST TECHNICAL UNIVERSITY

BY

RAMAZAN AYKUT SEZMEN

IN PARTIAL FULFILLMENT OF THE REQUIREMENTS
FOR
THE DEGREE OF MASTER OF SCIENCE
IN
MECHANICAL ENGINEERING

SEPTEMBER 2021

Approval of the thesis:

PERFORMANCE ANALYSIS OF GROOVED HEAT PIPES USING 3-D MULTI-CHANNEL THERMAL RESISTANCE NETWORK

submitted by **RAMAZAN AYKUT SEZMEN** in partial fulfillment of the requirements for the degree of **Master of Science in Mechanical Engineering Department, Middle East Technical University** by,

Prof. Dr. Halil Kalıpçılar
Dean, Graduate School of **Natural and Applied Sciences** _____

Prof. Dr. M. A. Sahir Arıkan
Head of Department, **Mechanical Engineering** _____

Prof. Dr. Zafer Dursunkaya
Supervisor, **Mechanical Engineering, METU** _____

Assoc. Prof. Dr. Barbaros Çetin
Co-supervisor, **Mechanical Engineering, Bilkent University** _____

Examining Committee Members:

Prof. Dr. Almıla Güvenç Yazıcıoğlu
Mechanical Engineering, METU _____

Prof. Dr. Zafer Dursunkaya
Mechanical Engineering, METU _____

Assoc. Prof. Dr. Özgür Bayer
Mechanical Engineering, METU _____

Assoc. Prof. Dr. Feyza Kazanç Özerinç
Mechanical Engineering, METU _____

Prof. Dr. Murat Köksal
Mechanical Engineering, Hacettepe University _____

Date: 07.09.2021

I hereby declare that all information in this document has been obtained and presented in accordance with academic rules and ethical conduct. I also declare that, as required by these rules and conduct, I have fully cited and referenced all material and results that are not original to this work.

Name, Surname: Ramazan Aykut Sezmen

Signature :

ABSTRACT

PERFORMANCE ANALYSIS OF GROOVED HEAT PIPES USING 3-D MULTI-CHANNEL THERMAL RESISTANCE NETWORK

Sezmen, Ramazan Aykut
M.S., Department of Mechanical Engineering
Supervisor: Prof. Dr. Zafer Dursunkaya
Co-Supervisor: Assoc. Prof. Dr. Barbaros Çetin

SEPTEMBER 2021, 77 pages

Heat pipes are phase change heat transfer devices that transfer high amounts of heat with low temperature differences compared to conventional cooling techniques due to their high thermal conductivity. Since heat pipes do not require any external power supply and not involve any moving parts, they are preferred for high reliability applications and in wide range of industrial applications from thermal management of electronics to space applications. Essentially, heat pipes use the advantage of occurring phase changes inside it and enable the movement of working fluid between its hot and cold ends. In the present study, thermal performance of flat grooved heat pipes (FGHP) for different design parameters and heat source and sink configurations are investigated. A three dimensional heat transfer model is developed using thermal resistance network analogy to simulate both conduction and phase change heat transfer. Coupled to thermal model, a one dimensional flow model is used to calculate change of radius of curvature and the velocity of the working fluid along the heat pipe's longitudinal axis. Developed heat transfer and flow models are solved in a coupled way and an iterative solution procedure is followed until the energy and

mass conservation are satisfied. Present three dimensional heat transfer model takes into consideration the lateral conduction heat transfer through the solid base material and allows to observe the effect of localized heat sources and sinks that do not entirely cover the width of FGHP. Crucial working parameters like wall temperatures all along the heat pipe, contact angle, vapor temperature and local hot spot regions are analyzed for local heat sources and sinks. Developed and validated models are used in a comprehensive study aiming to observe the effect of solid frame around the FGHP and in a parametric study investigating the effect of groove fin and width ratio for the same groove pitches.

Keywords: thermal resistance network, three-dimensional heat transfer, multi-channel, grooved heat pipe

ÖZ

ÜÇ BOYUTLU ÇOK KANALLI ISIL DİRENÇ AĞI KULLANILARAK OLUKLU ISI BORULARININ PERFORMANS ANALİZİ

Sezmen, Ramazan Aykut
Yüksek Lisans, Makina Mühendisliği Bölümü
Tez Yöneticisi: Prof. Dr. Zafer Dursunkaya
Ortak Tez Yöneticisi: Doç. Dr. Barbaros Çetin

Eylül 2021 , 77 sayfa

Isı boruları, yüksek ısı iletkenlikleri sayesinde bir ucundan diğer ucuna geleneksek soğutma yöntemlerine kıyasla daha düşük sıcaklık farkları ile yüksek ısı miktarları taşıyabilen faz değişimli ısı transfer cihazlarıdır. Dış bir güç kaynağına gereksinim duymamaları ve hareketli parça içermemeleri nedeniyle, elektroniklerin ısıl yönetiminden uzay uygulamalarına kadar çok geniş bir endüstride ve yüksek güvenilirlik gerektiren uygualamalarda tercih edilmektedirler. Temel olarak ısı boruları, olarak içinde gerçekleşen faz değişiminin avantajını kullanır ve sürekli olarak çalışma sıvısının sıcak ve soğuk uçlar arasındaki hareketine olanak sağlar. Bu çalışmada, düz oluklu ısı borularınınn (DOIB) farklı dizayn değişkenlerine ve ısı kaynağı ve soğutucuların dağılımlarını için ısıl perfomansı araştırılmıştır. Üç boyutlu ısı transfer modeli, ısıl direnç ağı kullanılarak hem ısı iletimi hem de faz değişimi ile gerçekleşen ısı transferini simüle etmek için geliştirilmiştir. Bir boyutlu akış modeli, ısı transfer modeli ile birleştirelerek eğrilik yarıçapının değişimi ve çalışma akışkanın hızı ısı borusu ekseni boyunca hesaplanmıştır. Geliştirilen ısı transfer ve akış modelleri enerji

ve kütle korunumu sağlanana kadar tekrarlı olarak birlikte çözülmüştür. Üç boyutlu ısı transfer modeli, katı temel malzeme üzerindeki yanal ısıl iletimi hesaba katar ve DOIB'nin tüm genişliğini kaplamayan bölgesel ısı kaynak ve emicilerin etkilerini gözlemleme imkanı sağlar. Farklı ısı kaynağı yerleşimleri için ısı borusu boyunca oluşan duvar sıcaklıkları, temas açısı, buhar sıcaklığı ve sıcak bölgeler gibi önemli çalışma değişkenleri analiz edilmiştir. Geliştirilen ve doğrulanan modeller kullanılarak DOIB etrafında yer alan katı çerçeve yapısının etkisini gözlemlemeyi amaçlayan bir çalışma ile oluk kanal ve kanatçık oranının etkisini inceleyen parametrik bir çalışma gerçekleştirilmiştir.

Anahtar Kelimeler: ısıl direnç ağı, üç boyutlu ısı transferi, çok kanallı, oluklu ısı borusu

To my parents and family in the future

ACKNOWLEDGMENTS

I would like to express my deepest gratitude to my advisor Prof. Dr. Zafer Dursunkaya for his continuous support and absolute guidance during my thesis study. Also I want to specially thank for his generous, encouraging and the kindest attitude towards me during our both technical and non-technical conversations. Without his constructive and precious comments, this thesis study could not be completed. It was really privilege for me to study under his guidance.

I would also like to thank my co-advisor Assoc. Prof. Dr. Barbaros Çetin for his vision that advancing the study and sharing his outstanding knowledge with me. The time I spent with him was always productive and valuable for me.

I wish to express my appreciation to ROKETSAN A.Ş. for giving me this opportunity and support my study. And also I would like to give my sincere thanks to Bülent Acar and my colleagues in Thermal Analysis and Test Unit for sharing their extensive technical and professional experience with me anytime I needed.

Lastly but most importantly, I would like to express gratefulness from the deep inside of my heart to my parents Sevtap Sezmen and Adnan Sezmen for their endless support and encourage not only for this study but in every part of my life.

TABLE OF CONTENTS

LIST OF TABLES

TABLES

LIST OF FIGURES

FIGURES

LIST OF ABBREVIATIONS

1D	1 Dimensional
2D	2 Dimensional
3D	3 Dimensional
A_d	Dispersion constant, J
c	Accommodation coefficient
h	Heat transfer coefficient, W/m^2·K
h_{fg}	Latent heat of evaporation, J/kg
k	Thermal conductivity, W/m·K
m	Molar mass of liquid, kg/mol
$\dot{m}$	Mass flow rate, kg/s
$m^{'}$	Mass flow rate per unit length, kg/m·s
$m^{''}$	Mass flow rate, kg/m^2·s
Me	Merit number
P_c	Capillary pressure, Pa
P_d	Dispersion pressure, Pa
P_l	Liquid pressure, Pa
P_v	Vapor pressure, Pa
$q^{''}$	Heat flux, W/m^2
R	Meniscus radius of curvature, m
R_u	Universal gas constant, J/mol·K
T	Temperature, K
u	Velocity in y-direction, m/s
	Greek Symbols
δ	Liquid film thickness, m

θ	Liquid-solid interface contact angle, Radian
μ	Dynamic viscosity, Pa·s
ν	Kinematic viscosity, m^2/s
ρ	Density, kg/m^3
σ	Surface tension, N/m
	Subscripts
$cond$	Condensation
$evap$	Evaporation
f	Fin
g	Groove
l	Liquid
lv	Liquid-vapor
pc	Phase change
s	Solid
v	Vapor

CHAPTER 1

INTRODUCTION

Fundamentally, heat pipes are devices that transport heat from a source to a sink with low temperature differences utilizing the phase change mechanisms occurring inside. Heat pipes are passive devices since they do not require any external power supply to operate. In addition being a passive device, heat pipes do not involve any moving parts inside. Heat pipes are able to transfer significant amounts of heat between its source and sink with low temperature differences compared to its base material [4]. All these properties make them reliable and one of the most important technique in thermal management applications. As a result of increasing demand on high heat dissipation in advanced power or electronic devices, traditional heat removing devices or techniques such as employing extended surfaces, forced convection etc. remain incapable in various applications. In recent years, heat transport devices that benefiting from latent heat evaporation draw interest of researchers and they are considered as an alternative heat transfer method to mentioned traditional ones. Therefore, heat pipes have been used as a favorable alternative [5] not only for thermal management of electronic components [6] but also in space applications [7], heating, ventilating and air-conditioning systems [8] and nuclear applications [9].

Heat pipes typically consist of a sealed container, working fluid inside this container and wick structure that generates the necessary driving force for the working fluid. Heat pipe is vacuumed in the manufacturing changed with the working fluid. During the operation of a heat pipe, working fluid continuously travels between its hot and cold ends which serve as evaporator and condenser, respectively. When heat pipe is heated at one end, it causes the evaporation of the working fluid. Due to the occurring pressure difference, the vapor moves towards the cooler end. Heat is removed in this

section and vapor condensates back to the liquid phase. As a result of phase change mechanism, liquid-vapor interface variation creates the necessary capillary pressure difference that is required for the liquid to travel back to evaporator section of the heat pipe. The movement of the working fluid inside an operating heat is illustrated in Fig 1.1. When there is a temperature difference, working fluid keeps moving between the two ends of the heat pipe and a significant amount of the heat is transferred with phase change instead of conduction through the solid container of the heat pipe.

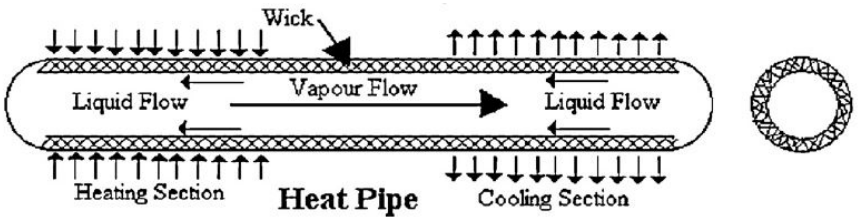

Figure 1.1: View of an operating heat pipe [2]

The container of the heat pipe provides a sealed and vacuumed environment for the working fluid. It is preferred that the material of the container have a high thermal conductivity to enhance the performance of the heat pipe. Also, it is crucial that container material and working fluid should be compatible.

Besides being compatible with the container material, there are some criteria to be aware of when selecting of working fluid. Operating temperature range of the heat pipe should be taken into consideration. A high latent heat of evaporation is favorable and important for the effectiveness and heat transport capacity of the heat pipe. In order to improve phase change, the selected working fluid should have good wettability on the wick structure. In addition, other chemical characteristics like toxicity, flammability should be thought especially in a laboratory environment. Some physical properties of commonly used working fluids and compatible materials are provided in Table 1.1. As a result, container material and working fluid needs to be selected properly by considering all the facts mentioned above. Otherwise, heat pipe may not operate in an effective way.

An important property, Merit number (Me), can be used for the working fluid selection since it is the indicator for the maximum heat transport capability of fluid based

Table 1.1: Some common working fluids and compatible materials [1]

Working Fluid	Melting point at Atmospheric Pressure (K)	Boiling point at Atmospheric Pressure (K)	Operating Temperature Range (K)	Compatible Materials	Incompatible Materials
Helium	1.0	4.2	2-4	-	-
Nitrogen	63.1	77.4	70-103	-	-
Methane	90.6	111.4	91-150	-	-
Ammonia	195.5	239.9	213-373	Aluminum, Stainless steel, Iron, Nikel	-
Acetone	180.0	329.4	273-393	Aluminum, Stainless steel, Copper, Brass, Silica	-
Methanol	175.1	337.8	283-403	Stainless steel, Iron, Copper, Brass,Silica	Aluminum
Ethanol	158.7	351.5	273-403	-	-
Water	273.1	373.1	303-550	Stainless steel, Copper, Silica, Nickel, Titanium	Aluminum, Inconel
Mercury	234.2	630.1	523-923	Stainless steel	Molybdenum, Nickel, Tantalum,Inconel, Titanium
Lead	600.6	2013.0	1670-2200	Tungsten, Tantalum	Molybdenum, Nickel, Inconel, Titanium, Niobium
Silver	1234.0	2485.0	2073-2573	Tungsten, Tantalum	Rhenium

on the capillary limit neglecting the vapor pressure loss and gravitational head.

$$Me = \frac{\rho \sigma h_{fg}}{\mu} \tag{1.1}$$

where ρ is the liquid density, σ is the liquid surface tension, h_{fg} is the latent heat of evaporation and μ is the liquid dynamic viscosity.

Necessary driving force for the circulation of the working fluid, namely the capillary force, is provided by the wick structure. Capillary action can be defined as the motion of the condensed liquid due to the adhesive attraction of dissimilar particles, and cohesive forces, attraction of similar particles, between the surface and the liquid. This action is achieved when the adhesive forces are greater than the cohesive forces of the fluid itself. Main wick structures used in commercial heat pipes are sintered, grooved and mesh wick type. The pictures illustrating the different wick structures are given Fig. 1-2. From top to bottom, sintered, mesh and grooved type wicks can be seen. In the pictures on the left, cross-section of the heat pipes having different wick structures are given. The pictures on the right show the interior mesh structure

of heat pipes.

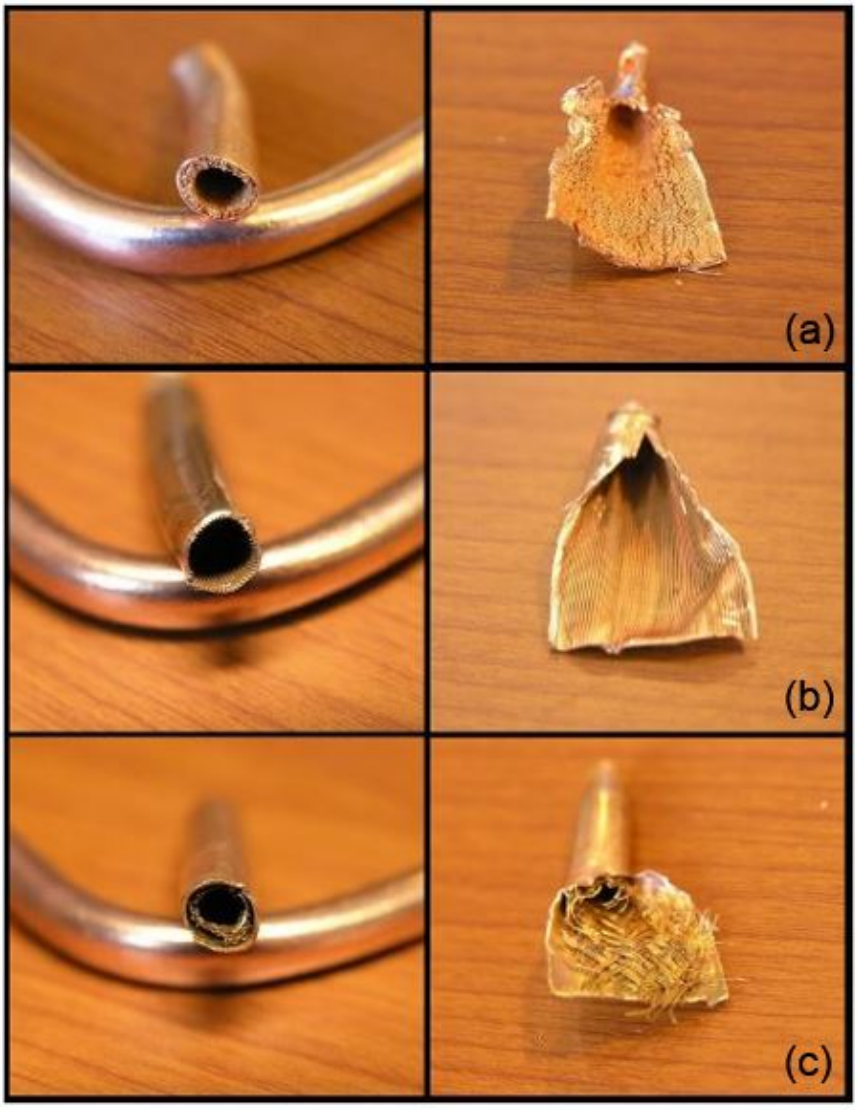

Figure 1.2: Section and cut-up views of different wick structures a) sintered wick, b) grooved wick, c) mesh wick [3]

Like working fluid and container material selection, selection of the wick structure also depends on application. The sintered wick is made by sintering a metal powder. This type of wick structure provides higher effective thermal conductivities compared to the other ones and suitable for using against gravity [10]. However, heat pipe with sintered wick has the highest cost compared to the other two common wick structure. Mesh wick structure is composed of a number of screen meshedyers applied to the inner wall of the heat pipe. Driving capillary force also can be provided by groove

wick structures. Cross-sections of the groove wick may have different shapes like square, rectangular, triangular and trapezoidal etc.. Heat pipes with groove wick structure have the lowest cost compared to sintered and mesh wick. Since shape, size and aspect ratio of the grooves have an important effect on the thermal performance of the heat pipe, they should be determined carefully by considering the application. Since the capability of generating capillary effect of groove wick is low compared to other wick structures [11], it is not desirable to use them against gravity. Grooved heat pipes are subjected to many experimental studies due to its ease of manufacturing. Depending on the application, it is possible to use combined wick structures to obtain necessary capillary force [12], [13]. In this thesis, thermal performance of heat pipes having groove wick structures are investigated.

1.1 Literature Review

As an effective way for removing heat from a source, heat pipes has been a subject in numerous studies and experiments. The first main idea for phase change heat transfer was introduced by A.M Perkins [1] with a device called a Perkins tube. The logic behind it is simply using continuous evaporation and condensation of working fluid inside a sealed tube. When the lower part of the chamber is heated, working fluid evaporates and flows through the cooler upper part of the chamber. Evaporated vapor condenses in this part and flows back to the evaporation region due to gravity. For the first time, heat pipe definition was appear in a paper by Groove et al. [14]. The authors explained the working principle and showed basic theoretical calculations. It was mentioned that returning of the condensate to the evaporator is accomplished by a suitable wick structure instead of gravity or by a pump. The authors stated that heat pipe could work in gravity-free conditions and be used in space applications. Several attempts to transfer more than 30 W/cm^2 through the heat pipe resulted in local over-heated areas due to dry-out of the wick structure. Dry-out phenomenon was considered as an important limitation on the proper operation of heat pipe. However, within certain limitations on the manner of use, heat pipe's equivalent thermal conductivity was evaluated to be substantially higher than any known metal.

In 1984, Cotter [15] introduced a model that approximates the maximum heat transfer

capacity of a triangular cross-section micro heat pipe. 1-D steady and incompressible flow equations in both liquid and vapor domains were solved to determine the maximum heat transfer capacity. The mass flow rates were used in local energy balance equations and integrated along the axial direction of heat pipe. Babin et al. [16], conducted both experimental and numerical studies to understand the operating characteristics of heat pipe with a rectangular cross-section. Using Young-Laplace equation, capillary pressure in the liquid domain was introduced to the model and variation in liquid-vapor interface radius was obtained using this relation. Container temperature of heat pipe was measured experimentally and compared with the numerical results. Beginning of the dry-out region was defined as where maximum temperature change occurred.

Various studies were conducted for different groove shapes like triangular shaped, V-shaped and Ω-shaped. Khrustalev et al. [17] and Peterson et al. [18] investigated heat transfer capacity of grooved heat pipes with triangular geometry. In both studies, liquid-vapor interfacial shear stress was taken into account and momentum equations were solved by using proper correlations both in liquid and vapor domains. In [18], total heat load was used for phase change and heat conduction in container material in heat pipe, conduction through the working fluid is neglected. Khrutalev and Faghri [17] calculated and used liquid film thickness and conduction through the micro regions to simulate heat transfer through the heat pipe. Pressure drops, maximum heat transport capacity and variation in liquid-vapor interface radius along heat pipe were calculated.

Kumar and Dasgupta [20] developed a model to calculate evaporation mass flow rates in meniscus and transition regions for V-shaped groove geometries. In this study, energy conservation equations were written for different unit liquid control volumes. The effect of apex angle and inclination on thermal performance of the heat pipe were investigated. The change in liquid-vapor interface curvature was also analyzed for different heat input values.

Suman and Dasgupta [21] compared the heat transport capacity of triangular and rectangular shaped heat pipes. In this study, authors developed a flow model for any polygonal shaped groove. Besides the flow model, mass transfer model was used

to calculate evaporated and condensed mass flow rates. However, axial variation of the temperature distribution was not considered in the heat balance of a unit control volume. A proposed numerical model used to calculate heat transfer capacities and predict dry-out point of both triangular and rectangular shaped heat pipes. Dry-out point and length of the dry-out region was predicted using the variation of liquid-vapor interface radius in the axial direction. Cross section geometry and contact angle were used to define minimum interface radius at the end of the evaporator region to determine dry-out performance of the heat pipe. It was concluded that triangular shaped heat pipes were able to carry more amount of heat compared to rectangular shaped ones. Effect of the surface tension, viscosity, contact angle, inclination angle and heat transport capacity were investigated in similar a study by Suman and Hoda [22] for heat pipes having V-shaped grooves.

Zhang [23] developed a 1-D model based on thermal resistances to optimize the performance of a heat pipe with Ω-shaped grooves. In this study effect of axial conduction is neglected and liquid-vapor interface radius was kept constant in evaporator and condenser regions. Neglecting variation in curvature radius might affect the results, especially when the pressure drop through the heat pipe is large. The effect of axial conduction might also be substantial, especially when the length of the adiabatic section is short. Other theoretical heat transfer and flow models were suggested by Chen et al. [24] to analyze maximum heat transport capacity of heat pipe with Ω-shaped grooves. In this study, effect of interfacial shear stress, variation in liquid-vapor interface radius and contact angle were taken into consideration. Obtained results for fluid pressure, velocity and liquid-vapor interface radius along the axial direction were compared with the experimental results.

Flat plate heat pipes with rectangular grooves have been investigated in numerous studies due to their ease of manufacture and experimentation. Do et al. [25] has developed a mathematical model to predict the thermal performance of a flat micro-heat pipe with a rectangular shaped wick structure. The influence of several operating parameters, such as the amount of liquid charge, the interfacial shear stress of the liquid-vapor and the contact angle, was investigated. It was concluded that some assumptions that used in the previous studies such as (i) evaporation and condensation were assumed to take place uniformly (ii) both evaporation and condensation occurred in

the adiabatic region and (iii) the container temperature was assumed constant may lead significantly misleading results for predicting thermal performance of heat pipe. It is recommended to consider the axial variation of the container temperature as well as the evaporation and condensation rates. Evaporation and condensation mass flow rates were calculated from relationships derived from kinetic theory. Results obtained from the developed model showed good agreement with the experimental data provided in [26] and [27].

Effect of filling ratio on the performance of a flat plate heat pipe was investigated in various studies both numerically and experimentally. Lips et al. [33], [34] conducted numerical and experimental analysis and investigated temperature fields and meniscus curvature radii in the FPHP for different heat loads, working fluid fillings and vapor spaces. Experimental results indicated that the filling ratio and the vapor space thickness have an important effect on the thermal performance of a flat grooved heat pipe. Filling ratio affected the meniscus curvature radius at the beginning of condensation which affected curvature radius variation along the heat pipe. Experimental results showed that the optimum filling ratio was in the range one 1–2.5 times the total volume of the grooves in all the cases. An experiment conducted in non-horizontal position showed that the dry-out of the evaporator occurred due to capillary limitations instead of nucleate boiling. The effect of the liquid-solid contact angle on performance of grooved heat pipe was investigated by Qu et al. [19] based on a 1-D steady-state model. Numerical results showed that the heat pipe with variable contact angle could transfer more heat compared to models that assumed a constant contact angle.

Rullière et al. [28] conducted an experimental study to determine thermal characteristics of two-phase heat spreaders (TPHS). Effect of different working fluids was investigated. 1-D two-phase flow model was developed to calculate meniscus radius, the liquid and vapor pressures and the liquid and vapor velocities along the TPHS. The developed model was based on momentum and Laplace-Young equations. The numerical results obtained without considering interfacial shear stress showed good agreement with the measured liquid-vapor interface radius. It was concluded that working fluid selection is important to obtain good thermal performance either in vertical or in horizontal orientation. Lefèvre et al. [29] developed a two-phase flow

and nodal temperature model to calculate liquid and vapor pressures and velocities, the meniscus curvature radius in the grooves and the temperature field in the heat pipe wall from the heat source to the heat sink. Flat grooved heat pipe was divided into several control volumes for the energy balance equations. The heat conduction in each cross section in liquid and solid regions was employed to obtain the thermal resistance, which was used to calculate axial temperature distribution along the heat pipe container. Then conservation and momentum equations were solved to obtain vapor velocities, the liquid and vapor pressures and the meniscus curvature radius are determined by the hydrodynamic model. This allowed to calculate transversal resistance by the evaporation and condensation models. Nodal temperatures were solved until the convergence criteria that the total transverse heat transfer rate from the evaporator beginning to the condenser end is equal to zero was satisfied for the nodal temperatures and the saturation temperature. The developed models were validated with experiments, where both wall temperatures and liquid-vapor meniscus radius were measured. In [38], Lips and Lefèvre used a similar model presented to [29] and investigated the effect of accommodation coefficient for different heat pipe materials. Also, condensate film on the fin top was compared with experimental results.

Odabaşı [30] investigated a flat micro grooved heat pipe with rectangular cross section. A model that solves the 3D heat transfer equations in both the solid and the liquid, coupled with a simplified 1-D momentum equation was presented. Both solid and liquid domains were modeled by 3D heat transfer equations. A simplified form of the momentum equation is formulated along the axis of the heat pipe to calculate the change of the liquid vapor interface radius along the heat pipe, which generates the capillary force required to direct the flow. The phase change heat transfer from the micro region is calculated using the equation obtained from the kinetic theory and the phase change heat transfer from both the micro region and the macro region is included in the analysis. Developed model was validated by comparing the results given in the literature. In this study, it was concluded that only %1–20 of the heat input was transferred by conduction through the FGHP's solid material. The rest of the heat load was transferred via phase change.

The advantage of spreading heat and preventing the formation of temperature gradient and localized hot regions of heat pipes which especially have porous wick struc-

tures provide them wide range of applications in electronic cooling systems. Lefèvre and Lallemand [31] developed an analytical model that couples a 2D hydrodynamic model for both the liquid and the vapor phases inside a flat micro heat pipe and a 3D thermal model for flat micro heat pipe (MHP) with several electronic components simulating heat sources and heat sinks. In this study, constant heat flux boundary condition were used both in heat sink and heat source regions. In addition, convective heat transfer was defined at the heat pipe container surface. Darcy's law was employed to obtain the liquid velocity. The maximum heat transport capability of a flat MHP, proportion of heat flux that transport with conduction through heat pipe container were calculated. Moreover, it was shown that if an equivalent thickness copper plate were used instead of MHP, the maximum calculated temperature difference would be three times higher.

Revellin et al. [32] modified and experimentally validated the model that had been developed in [31]. The modification consisted of superposing two independent solutions in order to take into consideration the effect of the evaporation and condensation processes on the effective thermal conductivities of the porous medium which was considered as constant in [31]. Since correlations given in literature for effective conductivities of grooved heat pipes for evaporation and condensation were not suitable for the study, a numerical database was built to calculate effective conductivity in methanol filled groove structures. The effect of the vapor temperature and geometry on the amount of maximum heat transferred by the heat pipe was given.

Aghvami and Faghri [35] developed a simplified analytical thermo-fluid model including both vapor and liquid flows for flat heat pipes exposing different heat source and heat sink configurations. Temperature distribution was obtained by using two-dimensional steady-state heat conduction equation inside the container. Both in liquid and vapor region, steady, laminar and incompressible flow were solved for axial and transverse velocities and axial pressure distribution. The variation in location of heat source and heat sink regions resulted in changing of evaporation and condensation regions. In this study, four different heat source and sink configuration were investigated: (i) single heat source and heat sink at top, (ii) multiple heat sources and heat sink at top, (iii) heat source at the bottom and heat sink on the top and (iv) multiple heat sources and heat sink at the bottom and top. For FGHP's, the results showed

that the assumption that evaporation and condensation occurs uniformly in the axial direction and that evaporation occurs only in the evaporator section and condensation occurs only in the condenser section is valid only if the solid thermal conductivity is small and in the axial direction. wall conduction was negligible.

Beside analytical and numerical models developed for thermal performance analysis of flat plate heat pipes with multiple heat sources, an analytical study of cylindrical heat pipes with multiple heat sources was conducted by Shabgard and Faghri [37]. In this study, multi-dimensional heat conduction in the wall was coupled to the vapor and liquid flows inside the cylindrical heat pipe. Two different cooling conditions in the condenser, convective cooling and constant heat flux, were modeled. The results of the model were compared with both analytical and experimental results. It was concluded from a parametric study that axial heat conduction through the heat pipe might have an important effect on the pressure drops in the heat pipe. A more general analytical model for both flat and cylindrical heat pipes with several heat sources and heat sinks was presented in by Lefèvre [38]. In this study, analytical model presented in [31] for a flat plate heat pipe with one surface fully insulated generalized for different configurations: (i) flate plate heat pipe (FPHP) fully covered with a capillary structure, (ii) FPHP half covered with a capillary structure and (iii) cylindrical heat pipe. The main parameters for the capillary structure were equivalent thermal conductivity and permeability. Three-dimensional heat conduction equation in the heat pipe wall was solved by employing a Fourier series expansion. Two-dimensional balance equations for liquid and vapor regions were solved in a similar way.

Transient regime analysis of flat plate heat pipes with multiple heat sources and heat sinks was conducted by Sonan et al. [39]. A two-dimensional hydrodynamic model was developed to deal with fluid flow in wick and vapor flow area and a 3D thermal model coupled with hydrodynamic model was employed to calculate heat transfer through the heat pipe wall. The phase mechanism at liquid-vapor interphase was introduced to the solution procedure with the Clausius-Clapeyron law. The steady-state results of developed model were compared with the published results in the literature. A very similar model was used by Harmand and Sonan [40] to calculate transient cooling performance and heat spreading effect of flat heat pipes connedted to multiple electronic components. The results of developed model were compared with

experimental and numerical results published in literature for both steady state and transient operation conditions. The thermal performance of heat pipe was compared with the solid copper plate. The results demonstrated that the flat heat pipe clearly operated as a thermal spreader which provided a more uniform temperature distribution than the solid copper plate. Another study that investigated both transient and steady-state performance of a flat heat pipe with multiple discrete heat sources was conducted by Vadakkan et al. [36] and a numerical analysis was performed. Three-dimensional flow for the vapor and wick regions and heat transfer equations along with conduction in the wall were solved. The evaporation and condensation rates were locally calculated using kinetic theory which required an empirical accommodation coefficient with an overall energy balance at the liquid-vapor interface.

In the current literature, there are very few studies conducted aiming to model and predict the thermal performance of multichannel heat pipes. Guichet et al. [41] proposed an analytical model in order to simulate thermal performance of a flat heat pipe and its cooling manifold and to validate the model it was tested experimentally. The channels of the studied heat pipe were linked by collectors at the bottom and the top. The top and the bottom of the multi-channel heat pipe was aiming to maintain the homogeneity of the phase flow. Complete thermal model comprised of different thermal resistances that simulate heater and heat pipe contact, wall conduction, two-phase of working fluid and convection at the condenser section of heat pipe. To estimate two-phase thermal resistances, pool boiling heat transfer correlations were used. The agreement between the experimental and analytical model data partially matched since the heat pipe thermal resistances estimated within 30% of error.

1.2 Objective and Description of the Current Study

As it is understood in the literature review section, a vast number of numerical and experimental studies have been conducted to understand and explain the basics and the working principle of the heat pipes. There are several geometrical and physical parameters that substantially affect the thermal performance of the heat pipes and the effect of each of them should be monitored. Numerical models respond quickly about the investigated parameters compared the experimental studies when the time con-

suming production process and the preparation of experimental setup are considered. Due to the assumptions and simplifications made in the numerical models, simulations may result in some misleading predictions due to the coupled disciplines and complex physics of the problem. Therefore, developed numerical models are need to be validated by experimental results obtained by the researcher or results provided in literature.

Main purposes and the contributions of this thesis study can explained as follows:

- Developing a fast and accurate model for the FGHP's that can provide rapid information about the thermal performance of the system.
- Extending developed model to a multi-channel model that enable to apply local heating and cooling boundary conditions and capture local hot spot regions through the heat pipe by taking into consideration the lateral heat conduction between the neighbor grooves.
- Conducting a comprehensive study investigating the effects of solid frame around the FGHP by advancing the multi-channel model.
- Performing a parametric study for different groove and fin width ratios with a constant groove pitch values in order to monitor performance of the FGHP and provide information for groove designs.

In Chapter 1, basic information about the heat pipe is given and working principle is explained. Previous numerical and experimental studies are summarized, objective and contributions of the present study is presented. In Chapter 2, modeling methodology both for heat transfer and flow models are explained in detail. In Chapter 3, the results of the validations studies of the developed half groove and multi-channel models are provided. In Chapter 4, the results and the findings of the comprehensive extended multi-channel model and the parametric study are given. In the final chapter, Chapter 5, the results of the current study are concluded, recommendations about the future works and extensible parts of the proposed models are discussed.

CHAPTER 2

THERMAL RESISTANCE ANALOGY BASED HEAT PIPE MODELING

Heat transfer and flow simulations of operating heat pipes have been extensively studied by the researchers and engineers for several years as mentioned in the literature review. Because of its complex physics of the heat pipes, special treatments and methodologies must be implemented to conduct a performance analysis. While numerically modeling an operating heat pipe, techniques for phase change phenomena, fluid flow and heat transfer modeling should be developed.

Before designing or just using a commercially available heat pipe for a particular engineering application, a detailed and realistic performance analysis should be conducted. The effect of different groove geometries, heater-cooler geometries and places, heat loads etc. should be investigated to design a reliable heat management system. Due to the reasons mentioned in the paragraph above, obtaining both cost effective and realistic solutions are not always the case. To handle this, a solution methodology is suggested and validated in the current study.

In this chapter, two different heat transfer modeling approaches for various loading configurations, fluid flow modeling, phase change modeling, coupled and iterative solution procedure and validation study of the suggested models are provided and explained in detail.

2.1 Thermal Resistance Networks

In the current study, developed heat transfer model is constructed based on thermal resistance networks to calculate heat transfer rates through the heat pipe both in solid

and liquid domains. Two different heat transfer models are generated. One of them benefits from the symmetry and simulates half groove geometry, if heat load and groove geometry allow the use of symmetry boundary conditions. The second model is the extended version of the half groove thermal resistance network to multi-channel thermal network. In the following subsections, construction details of the heat transfer models are explained.

2.1.1 Half Groove Resistance Network

In this thermal resistance network, using the symmetry of the groove geometry, heat load and heat sink conditions, the problem is simplified to half groove thermal resistance network. Geometrical illustration of the system and used parameters are given in Fig. 2.1. In provided figure, Fig. 2.1, grey and blue parts represent solid and liquid domains, respectively. Physical interpretations of the parameters is tabulated in Table 2.1.

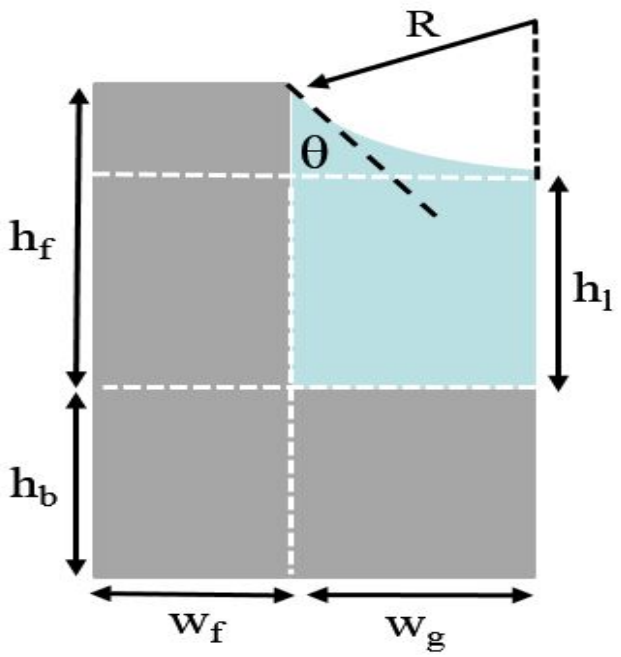

Figure 2.1: Groove geometry

Heat pipe divided into several slices including the evaporation, condensation and adiabatic regions. To simulate the effect of axial heat conduction, each slice along the

Table 2.1: Physical interpretations of the groove parameters

w_f	Half fin width
w_g	Half groove width
h_f	Fin height
h_b	Base height
h_l	Liquid height in groove
$\mathcal{R}$	Liquid-vapor interface radius
θ	Contact angle

heat pipe axis connected to each other with axial thermal resistances, R_a. Also the lateral heat conduction in the solid half groove domain is accounted by using a thermal resistance, R_b. Because of the different mechanisms involve in evaporation and condensation process, distinct resistance networks are utilized for them. Thus, the model is able to capture whether evaporation or condensation occurs in each particular slice and uses the corresponding network resistance. Every slice has five temperature nodes and energy conservation equations are written for all nodes in the network. Thermal resistance networks for evaporation and condensation are given Fig. 2.2 and 2.3, respectively.

$$R_1 = R_6 = \frac{h_b}{k_s w_f \Delta y} \tag{2.1}$$

$$R_2 = R_7 = \frac{h_b}{k_s w_g \Delta y} \tag{2.2}$$

$$R_3 = R_8 = \frac{h_l}{k_s w_f \Delta y} \tag{2.3}$$

$$R_4 = R_9 = \frac{h_l}{k_l w_g \Delta y} \tag{2.4}$$

$$R_5 = \frac{\Delta T}{\Delta y \int \dot{m}''_e h_{lv} ds} \tag{2.5}$$

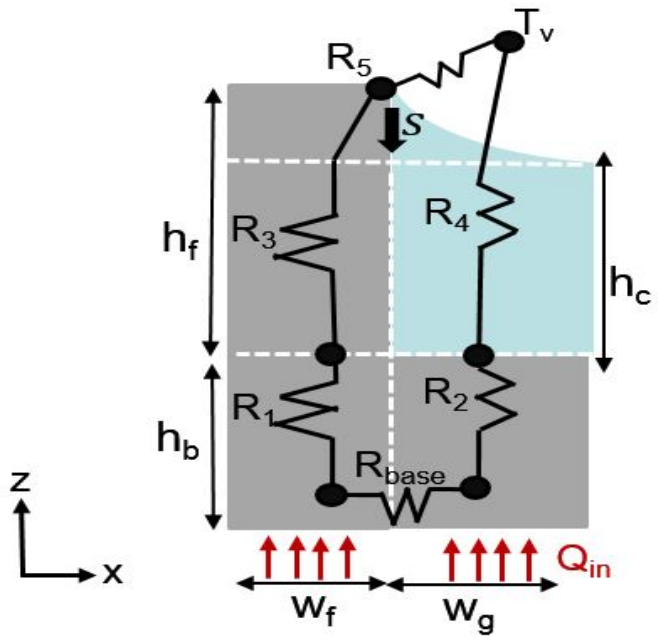

Figure 2.2: Evaporation section thermal resistance network

$$R_{10} = \frac{\Delta T}{\Delta y \int \dot{m}_c'' h_{lv} ds} \tag{2.6}$$

$$R_{conv,1} = \frac{1}{h w_f \Delta y} \tag{2.7}$$

$$R_{conv,2} = \frac{1}{h w_g \Delta y} \tag{2.8}$$

$$R_{base} = \frac{(w_f + w_g)/2}{k_s h_b \Delta y} \tag{2.9}$$

where Δy, h, T_v and T_∞ are unit slice length along axial direction, convective heat transfer coefficient between the heat pipe and heat sink, vapor temperature and ambient temperature, respectively. Heat transfer takes place in the fin top of the evaporation section is neglected because convection heat transfer at this area is negligible compared to evaporation heat transfer. The 2D evaporation heat transfer in the fin top corner is introduced to the model by using thermal resistance R_5.

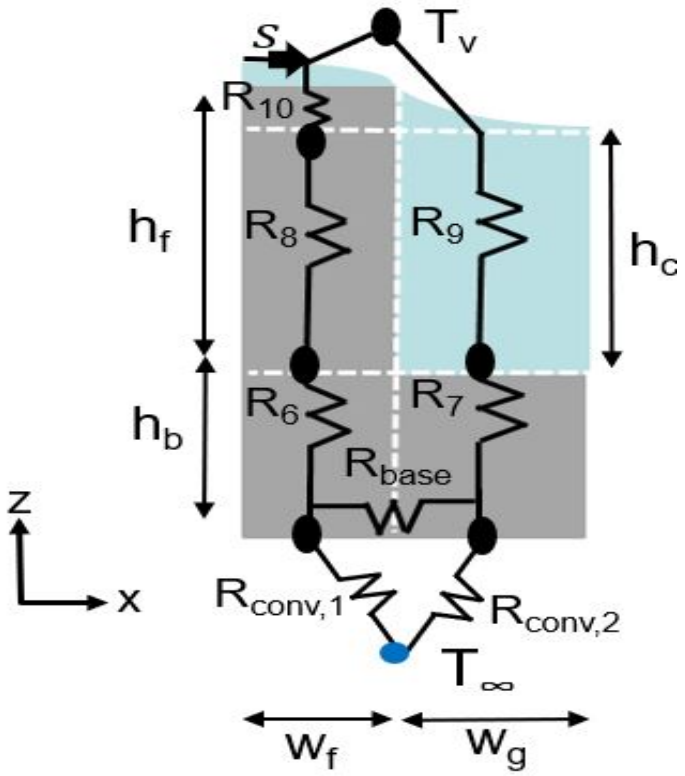

Figure 2.3: Condensation section thermal resistance network

In the condensation region, heat transfer at the fin top region is taking into consideration by using R_{10}. The details and the calculation methods of the phase change heat transfer resistances namely R_5 and R_{10} are given in Section 2.2.

2.1.2 Multi-Channel Resistance Network

In real life applications, heat pipes may not be exposed to symmetrical and uniformly distributed heat sources. Therefore, to conduct a more realistic and performance analysis, half groove thermal resistance network is extended to a multi-channel model. To do this, corresponding nodes in the half groove resistance networks are connected to its neighbor grooves with thermal resistances, R_g. Expression for the R_g is given in Eqn. (2.10):

$$R_g = \frac{w}{k_s h_b \Delta y} \tag{2.10}$$

where w represents the half fin w_f or half groove width w_g. Extended multi-channel model takes into account the effect of lateral heat transfer between channels and allows to apply the localized heat source and heat sink which is encountered in real life thermal management applications frequently. Extended model is able to capture local hot spot regions through the heat pipe, thus effect of the local hot spot region on heat pipe performance can be analyzed. Also, neighbor slices in the longitudinal direction are connected to each other with thermal resistance, R_a which is given in Eqn. (2.11). Constructed multi-channel thermal resistance network is given in Fig. 2.4.

$$R_a = \frac{\Delta y}{k_s(h_b + h_f)w_f} \tag{2.11}$$

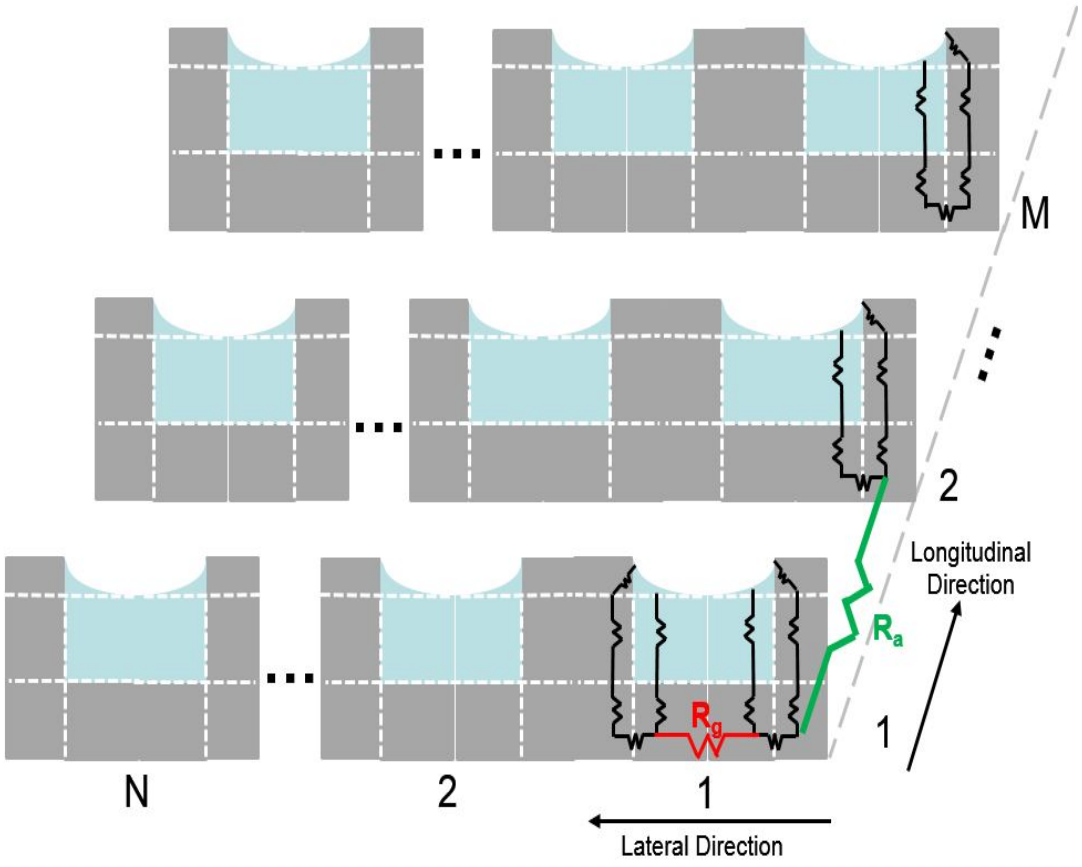

Figure 2.4: Multi-channel thermal resistance network

2.2 Phase Change Modeling

The advantages and working principles of heat pipes are based upon the occurrence of phase change mechanisms. Phase change is changing of a substance state as a result of releasing or absorbing energy from its surrounding. The amount of energy released or absorbed during the phase of a certain amount of substance, for instance mole, gram, kilogram, is defined as latent heat. If the substance state changes from liquid to vapor, the process is called "evaporation" and reverse of it i.e. from vapor to liquid, called "condensation". During the operation of heat pipe, evaporation and condensation occur as long as there is a temperature difference. Since significant amount of heat is transferred via the phase change compared to overall heat transferred, understanding the physics behind the evaporator and condensation phenomena is vital to predict thermal performance correctly. In this section, evaporation and condensation models used in this study are explained.

2.2.1 Evaporation Modeling

Evaporation is mainly a process that takes place in the liquid surface if the liquid molecules have sufficient energy to overcome the intermolecular forces at the liquid-vapor interface to change thestate from liquid to gas. Amount of energy of the liquid molecules required to suppress intermolecular forces is directly related to temperature. With increasing temperature, accruing rate of evaporation increases.

In the case of heat pipes, when one end is heated, evaporation starts to take place as a result of increasing energy of liquid molecules. Specifically in the grooved heat pipe (GHP) case, evaporation takes places in the grooves. The domain where this phenomena occurs can be divided into three sub-regions according to dominant effects [46]:

i *Intrinsic meniscus region*, the region where intermolecular forces are very weak due to the thick liquid layer compare to other two region and can be neglected. In this region, capillary force is dominant and satisfy the equilibrium.

ii *Evaporation thin-film region*, the region where capillary and intermolecular forces are both dominant

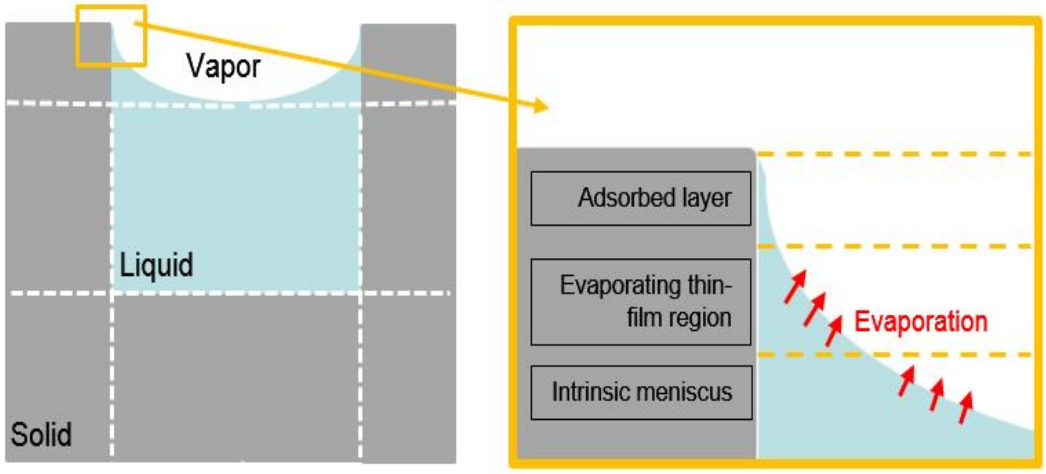

Figure 2.5: Evaporation domain and subregions

iii *Adsorbed layer*, liquid layer thickness drops to order of nano-scale and intermolecular forces between the liquid molecules and the groove wall become dominant. It is assumed that heat flux and mass transfer do not observed in this region.

At the liquid-vapor interface regions mentioned above, conservation equations should be satisfied. In meniscus macro region, the capillary force created by curvature is given by the Young-Laplace equation, by neglecting radius of curvature in axial direction since it is very high compare to radius in cross-section area:

$$P_l - P_v = \frac{\sigma}{\mathcal{R}} \tag{2.12}$$

where σ is surface tension and $\mathcal{R}$ is the radius of curvature in the liquid-vapor interface region. In order to calculate mass of the evaporated working fluid, basically mass flux can be used as follow:

$$q_l^{''} - q_v^{''} = m_e^{''} h_{lv} \tag{2.13}$$

Although thin film region is small compare to meniscus macro region, due to the low thermal resistance in corresponding area, high heat and mass fluxes are observed [42].

In this evaporation phase change model, kinetic theory is employed to calculate the mass flux due to the phase change:

$$m_e^{''} = a(T_{lv} - T_v) + b(P_l - P_v) \tag{2.14}$$

where

$$a = \frac{2c}{2-c}\left(\frac{M}{2\pi R_u T_{lv}}\right)^{1/2}\left(\frac{M P_v h_{lv}}{R_u T_{lv} T_v}\right) \tag{2.15}$$

$$b = \frac{2c}{2-c}\left(\frac{M}{2\pi R_u T_{lv}}\right)^{1/2}\left(\frac{P_v V_l}{R_u T_{lv}}\right) \tag{2.16}$$

where c is the accommodation coefficient, M is the molecular weight, R_u is the universal gas constant, h_{lv} is the latent heat of evaporation, T_v is vapor temperature, T_{lv} is liquid- vapor interface temperature, V is molar volume of liquid phase, P_v is vapor pressure and P_l is liquid pressure.

A coordinate system is defined to use in the solution of kinetic theory. The created coordinate system can be seen in Figure 2.6. Origin of the created system is placed on the transition region between meniscus macro region and thin-film region in the direction of s. On the other hand, in direction of n, origin is placed on the groove wall. Thickness of the liquid layer in the thin-film region is indicated as δ and θ indicates the angle between the groove wall and the liquid, namely contact angle.

Since the thermal resistance represented the evaporation phase change, R_5, is calculated between the groove wall temperature T_w, and vapor temperature T_v, liquid-vapor interface temperature T_{lv} should be eliminated from the Eqn. (2.14). To do this, mass flux between the liquid-vapor interface and groove wall can be written in terms of heat flux in this region:

$$m_e^{''} = a(T_{lv} - T_v) + b(P_l - P_v) = k_l \frac{T_w - T_{lv}}{\delta h_{lv}} \tag{2.17}$$

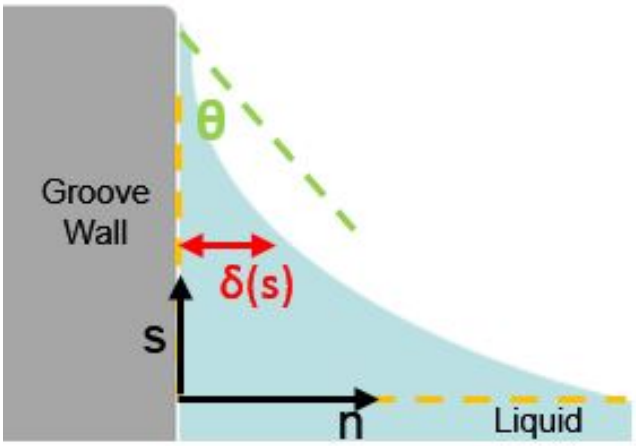

Figure 2.6: Coordinate system created for evaporation modeling

From Eqn(2.17), T_{lv} can be obtained as:

$$T_{lv} = \frac{k_l T_w/(\delta h_{lv}) + aT_v + b(P_v - P_l)}{a + k_l/(\delta h_{lv})} \tag{2.18}$$

By substituting Eq. (2.18) into Eq. (2.17), evaporation mass flux can be written in terms of the groove wall temperature T_w, and vapor temperature T_v:

$$m_e'' = \frac{a(T_w - T_v) + b(P_l - P_v)}{1 + a\delta h_{lv}/k_l} \tag{2.19}$$

Similar to mass balance, a force balance on the interface results in an expression for pressure:

$$P_v = P_l + P_c + P_d \tag{2.20}$$

where P_c is capillary pressure and P_d is disjoining pressure. P_d is defined as:

$$P_d = \frac{A_d}{\delta^3} \tag{2.21}$$

where A_d is the dispersion constant. Young-Laplace equation can be used to define

capillary pressure, P_c in terms of the liquid film thickness:

$$P_c = \sigma \frac{d^2\delta/ds^2}{(1+(d\delta/ds)^2)^{3/2}} \tag{2.22}$$

Relations written for P_d and P_c can be substituted to pressure balance equation Eq. ((2.20)). Also it should be noticed that during the evaporation process, since there is no considerable change occurring in P_v, it is assumed constant. By taking the derivative of pressure balance equation in the interface region with respect to delta(s):

$$\frac{dP_l}{ds} - \frac{3A_d}{\delta^4}\frac{d\delta}{ds} + \frac{\sigma d^3\delta/ds^3}{(1+(d\delta/ds)^2)^{3/2}} - \frac{3\sigma(d^2\delta/ds^2)^2}{(1+(d\delta/ds)^2)^{5/2}}\frac{d\delta}{ds} = 0 \tag{2.23}$$

Considering the flow from the macro region as one-dimensional fully developed in s-direction:

$$\frac{dP_l}{ds} = \mu \frac{d^2u_l}{dn^2} \tag{2.24}$$

Subjected to following boundary conditions

$$u_l = 0 \qquad \text{at} \qquad n = 0 \tag{2.24a}$$

$$\frac{du_l}{dn} = 0 \qquad \text{at} \qquad n = \delta \tag{2.24b}$$

Using the equation Eq. (2.24) and boundary conditions given in Eq. (2.24a) and Eq. (2.24b), liquid velocity in the direction of groove wall, can be obtained as:

$$u_l = \frac{1}{\mu}\frac{dP_l}{ds}(n^2/2 - \delta n) \tag{2.25}$$

Evaporation mass flow rate per unit length can be get by integrating liquid velocity Eq. (2.25) through the liquid film thickness:

$$m_e^{'} = \rho_l \int_0^{\delta} u_l dn \tag{2.26}$$

In order to obtain evaporation mass flux, Eq. (2.26) can be differentiated with respect to s. After the differentiation, considering the Eq. (2.23), evaporation mass flux rate can be obtain in terms of liquid film thickness δ(s):

$$m_e{}'' = -\frac{d}{ds}\left[\frac{\delta^3}{3\nu}\left(\frac{3A_d}{\delta^4}\frac{d\delta}{ds} - \frac{\sigma d^3\delta/ds^3}{(1+(d\delta/ds)^2)^{3/2}} + \frac{3\sigma(d^2\delta/ds^2)^2}{(1+(d\delta/ds)^2)^{5/2}}\frac{d\delta}{ds}\right)\right] \quad (2.27)$$

Rearranging Eq. (2.19) and Eq. (2.27) yields to Eq. (2.28) and boundary conditions given in Eq. (2.28a - 2.28f):

$$\begin{aligned} m_e{}'' &= \frac{a(T_w - T_v) + b(P_l - P_v)}{1 + a\delta h_{lv}/k_l} \\ &= -\frac{d}{ds}\left[\frac{\delta^3}{3\nu}\left(\frac{3A_d}{\delta^4}\frac{d\delta}{ds} - \frac{\sigma d^3\delta/ds^3}{(1+(d\delta/ds)^2)^{3/2}} + \frac{3\sigma(d^2\delta/ds^2)^2}{(1+(d\delta/ds)^2)^{5/2}}\frac{d\delta}{ds}\right)\right] \end{aligned} \quad (2.28)$$

$$\delta = \delta_0 \quad \text{at} \quad s = 0 \quad (2.28a)$$

$$d\delta/ds = \tan\theta \quad \text{at} \quad s = 0 \quad (2.28b)$$

$$P_v - P_l = \sigma/R \quad \text{at} \quad s = 0 \quad (2.28c)$$

$$d(P_v - P_l)/ds = 0 \quad \text{at} \quad s = 0 \quad (2.28d)$$

$$m_e^{''} = 0 \quad \text{at} \quad s = l \quad (2.28e)$$

$$P_d = \frac{\sigma}{\mathcal{R}}10^{-5} \quad \text{at} \quad s = 0 \quad (2.28f)$$

In boundary condition Eq. (2.28f), since s=0 corresponds the section where transition from macro region to the thin-film micro region, it is assumed that dispersion pressure P_d is equal to 1/10^5 of the capillary pressure, P_c.

In order to use evaporated mass flux in the corresponding evaporation thermal resistance, namely R_5, heat flux and heat transfer rate in thin-film micro region defined as:

$$q^{''} = h_{lv} m_e{}'' \quad (2.29)$$

$$q = \Delta z \int_0^l q^{''} ds \quad (2.30)$$

where Δz is the unit slice length in the direction of groove axis. Substituting Eq. (2.19) into Eq. (2.30), heat transfer rate, q can be obtained in terms of groove wall temperature T_w, vapor temperature T_v and liquid film thickness δ(s):

$$q = \Delta z \int_0^l \frac{a(T_w - T_v) + b(P_l - P_v)}{1 + a\delta h_{lv}/k_l} h_{lv} ds = \frac{T_w - T_v}{R_5} \tag{2.31}$$

Using the Eq. (2.31), thermal resistance represents the heat transfer through the evaporation phase change is obtained as:

$$R_5 = \frac{T_w - T_v}{\Delta z \int_0^l \frac{a(T_w - T_v) + b(P_l - P_v)}{1 + a\delta h_{lv}/k_l} h_{lv} ds} \tag{2.32}$$

2.2.2 Condensation Modeling

Other phase change type observed during the operation of heat pipes is condensation. Condensation is the reverse process of the evaporation where working fluid changes its state from gas to liquid. During condensation, heat carried by the latent heat of evaporation of the working fluid is released and removed by the heat sink. As heat is removed, working fluid changes its state. Similar to evaporation, significant amounts of heat is transferred in a particular region of the groove during condensation. Most of the condensation takes place at the top of the groove fin. This fin top region can be defined as the micro region for condensation. In this section, calculation of condensation heat and mass fluxes in micro region will be explained.

Similar to evaporation modeling, a coordinate system is defined in the cross-section. The created coordinate system and the cross-section of the condensation region can be seen in Figure2.7. Liquid film thickness and half fin width are denoted by δ(s) and w_f, respectively. The origin of the created coordinate system is placed on top of the fin.

Similar to evaporation modeling, condensation mass flux can be written in terms of

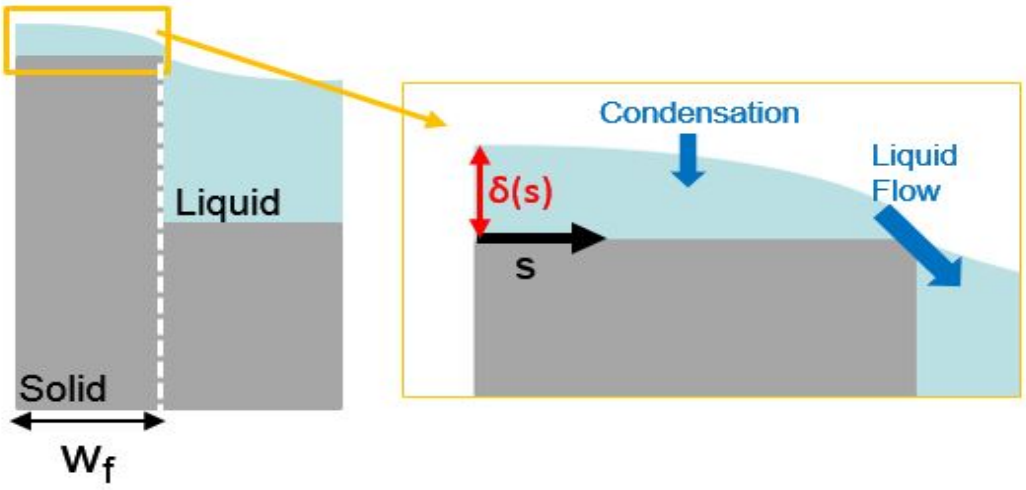

Figure 2.7: Coordinate system created for condensation modeling

the heat fluxes in the liquid-vapor interface:

$$q_l^{''} - q_v^{''} = m_c^{''} h_{lv} \tag{2.33}$$

Pressure balance in the liquid-vapor interface region can be written by using kinetic theory. It should be noted that different from the evaporation model, effect of the dispersion pressure is neglected due to the liquid film thickness in the fin top. Capillary pressure in balanced with the vapor and liquid pressures:

$$P_c = P_v - P_l \tag{2.34}$$

Since the variation of the liquid-film thickness in the fin top can be neglected, equations obtained in evaporation modeling Eq. (2.22) and (2.27) can be rearranged as:

$$P_v - P_l = P_c = \sigma \frac{d^2\delta}{ds^2} \tag{2.35}$$

$$m_c^{''} = \frac{\sigma}{3\nu}\frac{d}{ds}\left(\delta^3 \frac{d^3\delta}{ds^3}\right) = -\frac{a(T_w - T_v) + b(P_l - P_v)}{1 + a\delta h_{lv}/k_l} \tag{2.36}$$

A fourth order polynomial is fitted for the liquid film thickness profile on the fin top. Polynomial equation and corresponding boundary conditions are presented as follow:

$$\delta(s) \;=\; c_0 + c_1(s - w_f) + c_2(s - w_f)^2 + c_3(s - w_f)^3 + c_4(s - w_f)^4 \quad (2.37)$$

$$d\delta/ds = 0 \qquad \text{at} \qquad s = 0 \qquad (2.37a)$$

$$d^3\delta/ds^3 = 0 \qquad \text{at} \qquad s = 0 \qquad (2.37b)$$

$$d\delta/ds = -\tan(\pi/2 - \theta) \qquad \text{at} \qquad s = w_f \qquad (2.37c)$$

$$d^2\delta/ds^2 = 0 \qquad \text{at} \qquad s = w_f \qquad (2.37d)$$

Using the boundary conditions provided in Eq. (2.37a)-(2.37d), unknown coefficients c_1–c_4 are founded as:

$$c_1 = -\tan(\pi/2 - \theta) \qquad (2.38a)$$

$$c_2 = 0 \qquad (2.38b)$$

$$c_3 = \tan(\pi/2 - \theta)/2{w_f}^2 \qquad (2.38c)$$

$$c_4 = \tan(\pi/2 - \theta)/8{w_f}^3 \qquad (2.38d)$$

Remaining unknown coefficient, c_0 is obtained using a numerical iterative procedure. Integrating Eq. (2.36):

$$m_c^{'} = \frac{\sigma}{3\nu} 6c_0^3 c_3 = -\int_0^{w_f} \frac{a(T_w - T_v) + b(P_l - P_v)}{1 + a\delta h_{lv}/k_l} ds \qquad (2.39)$$

An objective function f defined and Secant method is used to obtain constant c_0. Once the c_0 is calculated, fourth-order liquid film thickness profile can be used for condensation mass flux.

$$f = \frac{\sigma}{3\nu} 6c_0^3 c_3 + \int_0^{w_f} \frac{a(T_w - T_v) + b(P_l - P_v)}{1 + a\delta h_{lv}/k_l} ds \qquad (2.40)$$

Once the liquid film thickness, δ, is obtained, condensation phase change heat transfer can be calculated as in the Eq. (2.41):

$$q = \Delta z \int_0^{w_f} \frac{a(T_w - T_v) + b(P_l - P_v)}{1 + a\delta h_{lv}/k_l} h_{lv} ds = \frac{T_w - T_v}{R_{10}} \tag{2.41}$$

Thermal resistance represents the heat transfer through the condensation phase change is obtained as:

$$R_{10} = \frac{T_w - T_v}{\Delta z \int_0^{w_f} \frac{a(T_w - T_v) + b(P_l - P_v)}{1 + a\delta h_{lv}/k_l} h_{lv} ds} \tag{2.42}$$

Zhang and Faghri [43] investigated condensation in a capillary groove using the volume of fluid (VOF) model. Condensation on the fin top and at the meniscus was modeled by employing continuity, VOF and energy equations. Similar to present study, due to the symmetry only half of the groove and the fin were included in the modeling. Governing equations were written for both the liquid and vapor regions. The effects of temperature drop, contact angle, surface tension and fin thickness on the condensation heat transfer were also investigated.

The results for liquid film thickness variation along the fin top compared with the results provided in the literature [30] and [43]. Physical and geometrical properties for the validation case is given in Table 2.2.

Fin top liquid film thickness variation for different temperature differences between the vapor and the wall and contact angles is compared with the results of Zhang and Faghri [43] and Odabaşı [30]. In Figure 2.8 liquid film thickness variation is given for contact angle 84 degrees and temperature difference $\Delta T = 10$ K. Difference between [43] and current study is about 26% at the fin top beginning. However, the difference in the heat flux would be lower since the resistance against the heat flow would be higher at the beginning and therefore the larger portion of heat will flow near the fin corner where liquid film thickness variation shows good agreement. Beside, the obtained results are well-suited with the Odabaşı's [30] since very similar approach used in this study.

In Figure 2.9, calculated liquid film thickness variations for different temperature

Table 2.2: Physical and geometrical properties used in liquid fin top thickness calculation

Half fin width (mm)	20×10^{-3}
Vapor temperature (K)	373
Vapor pressure (Pa)	1.03×10^{5}
Latent heat of evaporation (J/kg)	2.3×10^{6}
Density of liquid (kg/m^3)	1000
Dynamic viscosity (Pa· s)	2.79×10^{-4}
Surface tension (N/m)	58.9×10^{-3}
Thermal conductivity (W/m·K)	0.6
Molar mass of liquid (kg/mol)	18×10^{-3}
Accommodation coefficient	1

differences $\Delta T = 5$ and $\Delta T = 10$ K at a different contact angle 84 degree are compared with Odabaşı [30]. In both cases, results for film thickness variation in fin top show well agreement.

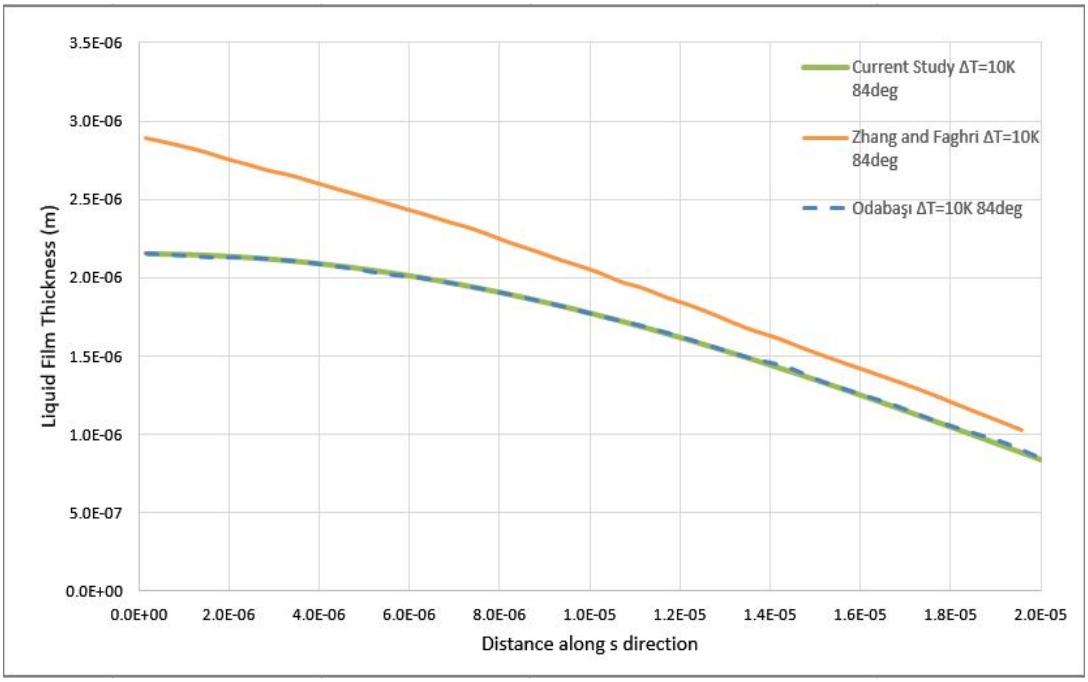

Figure 2.8: Liquid film thickness variation on fin top

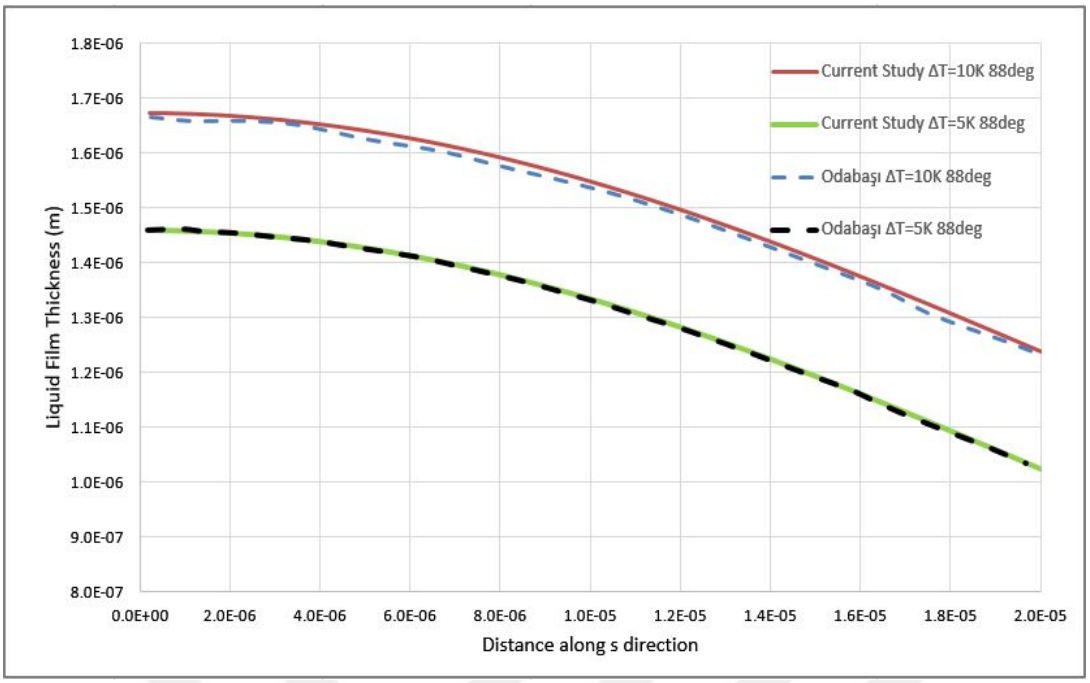

Figure 2.9: Liquid film thickness variation on fin top for different temperature differences

2.3 Fluid Flow Modeling and Mass Balance

During the operation of the heat pipe, working fluid must be circulate when there is a temperature difference exists between the evaporator and condenser end of the heat pipe. In order to maintain continuous circulation, capillary pumping pressure must be greater than the total pressure drop inside the pipe.

$$\Delta P_{c,max} \geq \Delta P_l + \Delta P_v + \Delta P_g \tag{2.43}$$

Aim of this section is calculating the liquid-vapor interface radius which is varying along the heat pipe during the operation. Since necessary driving force required for the flow generated by capillary pressure and its directly related with the interface radius, forces acting on working fluid is formulated. Unit control volume is used to write force balance along the axis of heat pipe. Relevant control volume is given in Figure 2.10.

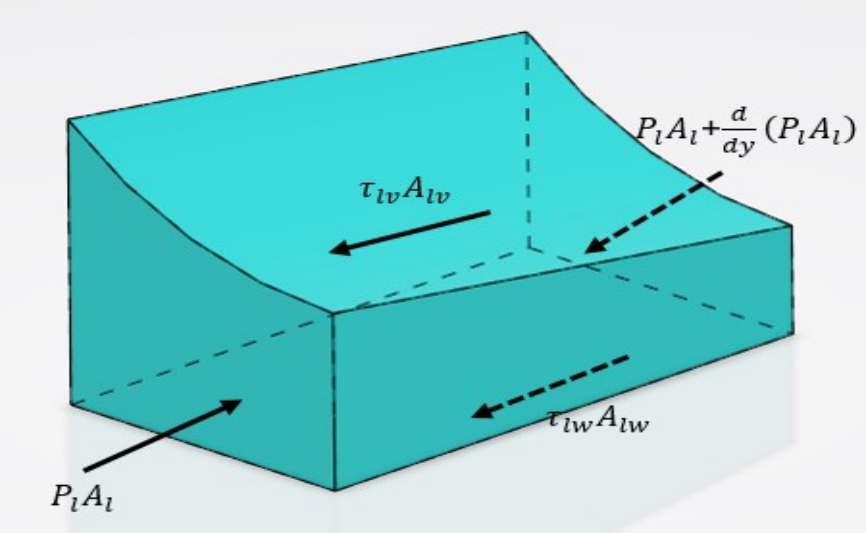

Figure 2.10: Force balance in liquid control volume

Force balance equation is written in Eq. (2.44) where A_{lw}, A_{lv}, τ_{lw} and τ_{lv} denote the liquid-wall interface area, liquid-vapor interface area, shear between liquid and wall and shear between liquid-vapor interface, respectively.

$$\rho_l \frac{d}{dy}\left(A_l u^2\right) dy = -\frac{d}{dy}\left(A_l P_l\right) dy + A_{lw}\tau_{lw} + A_{lv}\tau_{lv} \tag{2.44}$$

Due to the smooth transition between the evaporation and condensation regions and large volume of the vapor region liquid-vapor interface shear is neglected [29]. For the pressure term inside the Eq. (2.44), Young-Laplace relation is employed.

$$P_l = P_v - \frac{\sigma}{\mathcal{R}} \tag{2.45}$$

Assuming the constant vapor pressure along the heat pipe, derivative of Eq. (2.45) becomes:

$$\frac{dP_l}{dy} = -\sigma \frac{d}{dy}\left(\frac{1}{\mathcal{R}}\right) \tag{2.46}$$

Besides previous assumptions, by neglecting the variation in area of the liquid cross-

section and substituting Eq. (2.46) into Eq. (2.44), force balance equation yields to:

$$\rho_l \frac{d}{dy}\left(A_l u^2\right) = -\sigma A_l \frac{d}{dy}\left(\frac{1}{\mathcal{R}}\right) + L_{lw}\tau_{lw} \tag{2.47}$$

where L_{lw} represents the wetted perimeter at liquid-wall interface. In order to calculate shear at liquid-wall interface, following relation is used:

$$\tau_{lw} = 0.5\rho u^2 f = 0.5(Re \cdot f)\frac{\mu}{D_h}u \tag{2.48}$$

where D_h denotes the hydraulic diameter:

$$D_h = \frac{4A_l}{L_{lw}} \tag{2.49}$$

Appropriate correlation for the friction coefficient,f used in [25] is employed which is:

$$Re \cdot f = \frac{8r^2}{(1+r)^2(1/3 - (64/\pi^5 r)\tanh(\pi r/2))} \tag{2.50}$$

where r is stand for $r = h_f/w_g$, h_f is the fin height and w_g is half of the groove width. Remaining unknowns in force balance and shear equations are liquid cross-section, A_l and hydraulic diameter, D_h and they can be calculated by using the groove geometry provided in Figure 2.1.

$$A_l = 2w_g h_f - \left[(\pi/2 - \theta)R^2 - \frac{b^2}{\tan(\pi/2 - \theta)}\right] \tag{2.51}$$

$$D_h = \frac{4\left[2w_g h_f - (\pi/2 - \theta)R^2 + (w_g^2/\tan(\pi/2 - \theta))\right]}{2(w_g + h_f)} \tag{2.52}$$

Aiming to obtain liquid-vapor interface radius variation along the heat pipe, force and mass balance equations are solved iteratively. Liquid control volume showing the inlet and outlet masses illustrated in Figure 2.11.

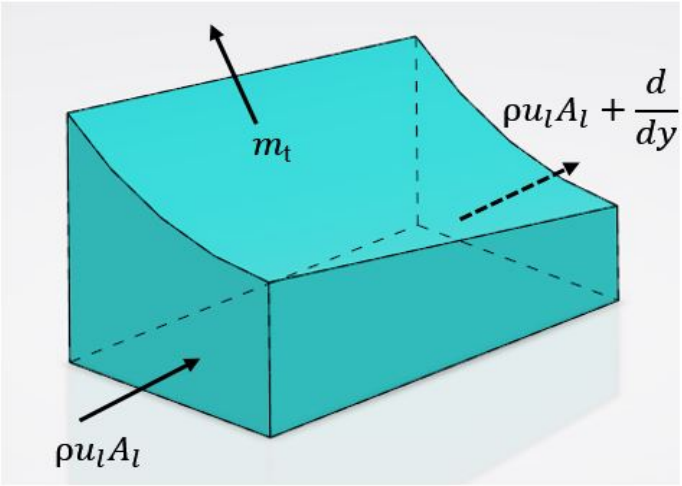

Figure 2.11: Mass balance in liquid control volume

$$\frac{d}{dy}\left(\rho_l u A_l\right) + \dot{m}_{pc} = 0 \tag{2.53}$$

In mass balance equation, $\dot{m}_{pc}$ indicates the total amount of phase change mass flow rate both in micro and macro regions. Iterative solution procedure used in [30] implemented to this study. Equations obtained for force and mass balances, Eq. (2.47) and Eq. (2.53, are discretized and solved iteratively by using secant method. At the beginning of the condenser section, liquid velocity u_1=0 and radius R_1 are used as initial values. For the next axial position, assumed R_2 is used in Eq. (2.47) to calculate liquid cross-section area. Mass balance equation Eq. (2.53) solved for liquid velocity using total mass change flow rates and calculated liquid cross-section area. Force balance equation solved for radius, R_2 and iteration continues until convergence is achieved. This iterative procedure repeated for the next axial position and liquid-vapor interface radius variation is obtained along the heat pipe.

2.4 The Solution Procedure

Developed numerical models which is analyzing the thermal performance of a flat grooved heat pipe solve coupled heat transfer equations and flow model in an iterative way. In this section, followed solution procedure is explained. A general procedure

is summarized in a flowchart is given in Figure 2.12. Groove geometry, material properties of solid and working fluid, evaporator, condenser and adiabatic lengths are provided as inputs to the model. In addition, thermal boundary conditions and loading conditions such as heat transfer coefficient, heat flux and ambient temperature must be defined for the solution. In order to start the iterative solution procedure, estimations for the vapor temperature T_v and wall temperature distribution T_w along the heat pipe are made since total phase change mass flow rate is function of both wall and vapor temperatures. Also contact angel at the beginning of the condenser region (contact angle at the end of the heat pipe) must be defined for the particular solution.

The solution procedure start with solution of phase change mass flow and fluid flow equations with the initial guesses as explained in Section 2.3. The variation of the liquid-vapor interface radius and contact angle along the heat pipe are obtained as a result of the flow model solution. Obtained radius variation used in the calculation of corresponding thermal resistances. Once the thermal resistance network is constructed, it is solved for the new temperature, ${T_w}^{\text{new}}$ distribution. Obtained temperature distribution are used as input for the flow model until the converge criteria for the wall temperature is satisfied. For the T_v convergence, equality of total evaporated and condensated masses are checked. Until the conservation of mass criteria is satisfied, vapor temperature T_v is updated. For the updated vapor temperature value, all solution procedure is repeated until converge criteria is satisfied.

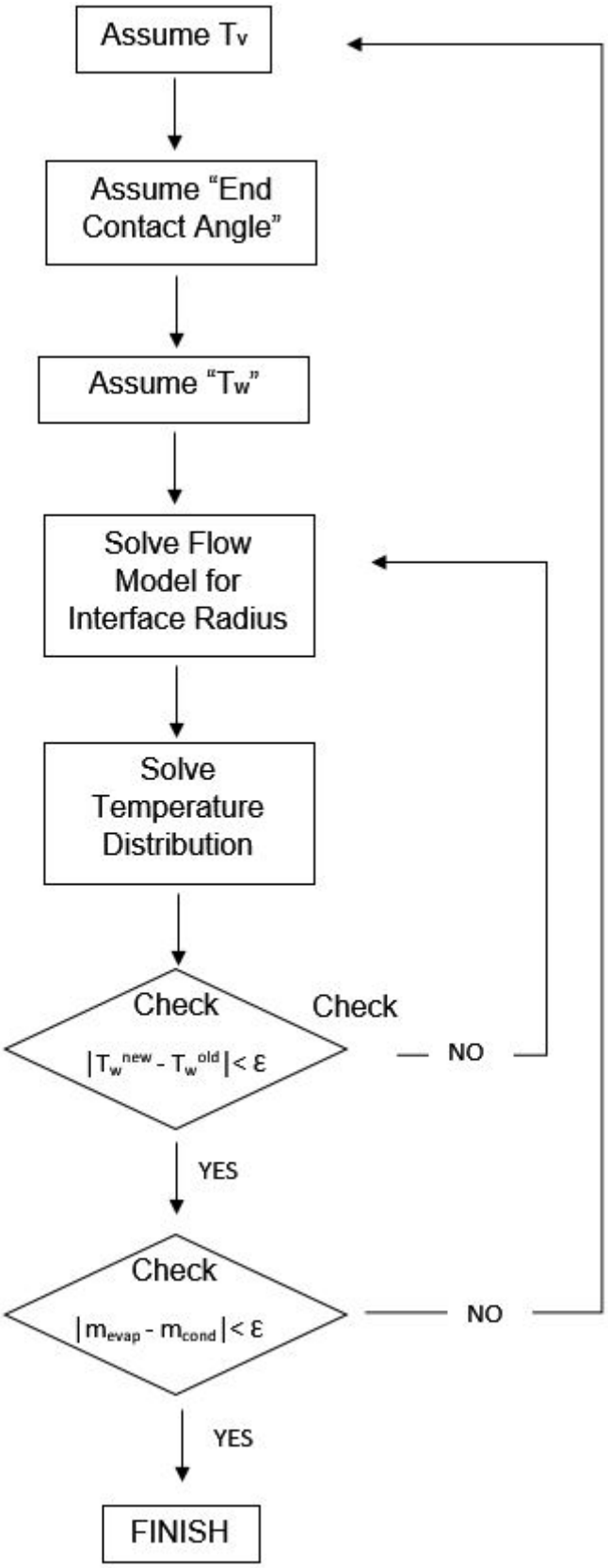

Figure 2.12: Flowchart of the numerical model solution procedure

CHAPTER 3

VALIDATION OF MODELS

In this section, results of current study is compared with the numerical and experimental studies available in the literature. Comparison results for the half groove and multi-channel models are provided in the following sections.

3.1 Validation Results for the Half Groove Model

In order to validate the developed half groove model, results of current study is compared with the numerical and experimental study provided by Lefèvre et al. [29] and Saygan [45] and with the numerical studies by Odabaşı [30] and Gökçe [44]. The parameters used in the validation are liquid-vapor interface radius and liquid velocity for the flow model and wall temperature for the heat transfer model.

In the first validation study, results of the Lefèvre et al. [29], Odabaşı [30] and Gökçe [44] are used. In this study, solid container material and working fluid was copper and methanol, respectively. Physical and geometrical properties used in the first validation study is provided in Table 3.1.

The first essential parameter used in the validation study is liquid-vapor interface radius variation. Since it creates the driving force for the flow inside and has major effect on the phase change heat transfer especially in thin film and fin top regions, calculation of the interface radius variation along the heat pipe is critical for both flow and heat transfer model. Interface radius variation is plotted in Fig 3.1.

Although different methodologies used in the studies, calculated interface radius variation is very similar to all validations studies as seen in Fig. 3.1. Odabaşı [30] and

Table 3.1: Physical and geometrical properties used in the validation study

Length of FGHP (mm)	230
Half groove width, w_g (mm)	0.2
Half fin width, w_f (mm)	0.2
Base height, h_b (mm)	2
Fin height, h_f (mm)	0.38
Length of heat source region (mm)	190
Length of heat sink region(mm)	30
Heat load (W/m^2)	5000
Heat transfer coefficient (W/m^{2}K)	2100
Ambient temperature (°C)	50

Lefèvre et al. [29] used 1-D flow model approach to simulate liquid flow inside the grooves. On the other hand, Gökçe [44] calculated interface radius directly using the CFD results in 3-D domain. In the current study, very similar approach to Odabaşı's study [30] is implemented for the flow modeling as explained in Section 2.3. In all cases, interface radius variations are well-suited with each other.

Another parameter used in the validation study is liquid velocity inside the groove. Liquid velocity distribution is given in Fig 3.2. At the ends of the heat pipe, liquid velocity is zero. It reaches the maximum value at the transition region between evaporation and condensation zones.

Calculated temperature variation is compared with the findings of the all studies used in the first validation study. In all three studies, calculated vapor temperatures are very similar and between 69.2°C and 70.0°C.

As seen in Fig. 3.3, wall temperature distributions show similar trends in current study, Odabaşı [30] and Gökçe [44]. However, in Lefèvre's study [29], maximum temperature difference along the heat pipe is smaller than the current study. This difference may show up due to the different modeling techniques used in the phase change and heat transfer modeling. In the current study, Gökçe [44] and Odabaşı [30] similar micro region phase change methodology is followed. Beside, Lefèvre et.

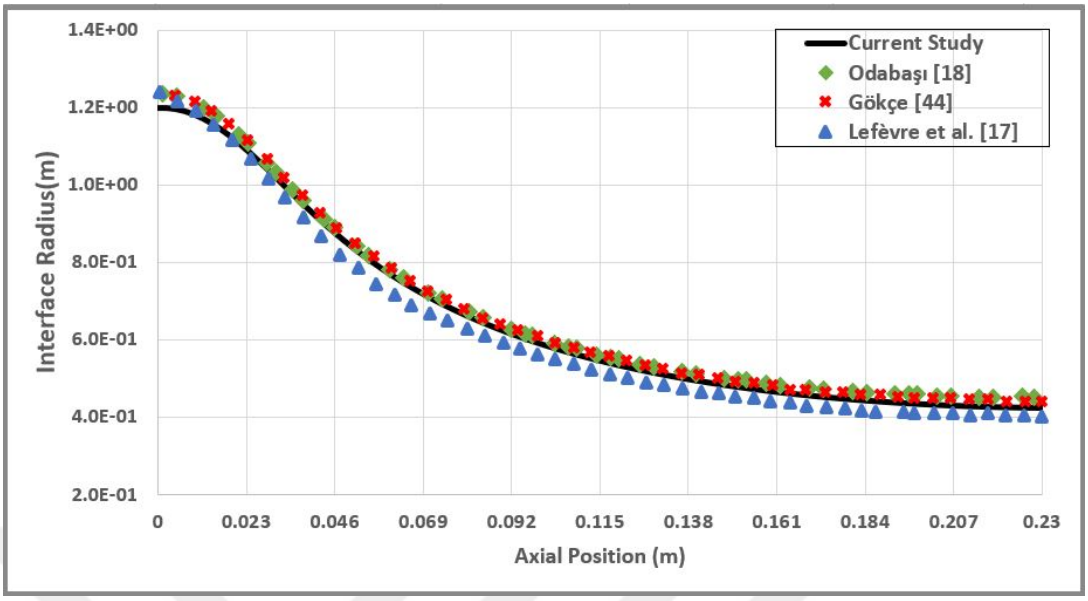

Figure 3.1: Liquid-vapor interface radius variation

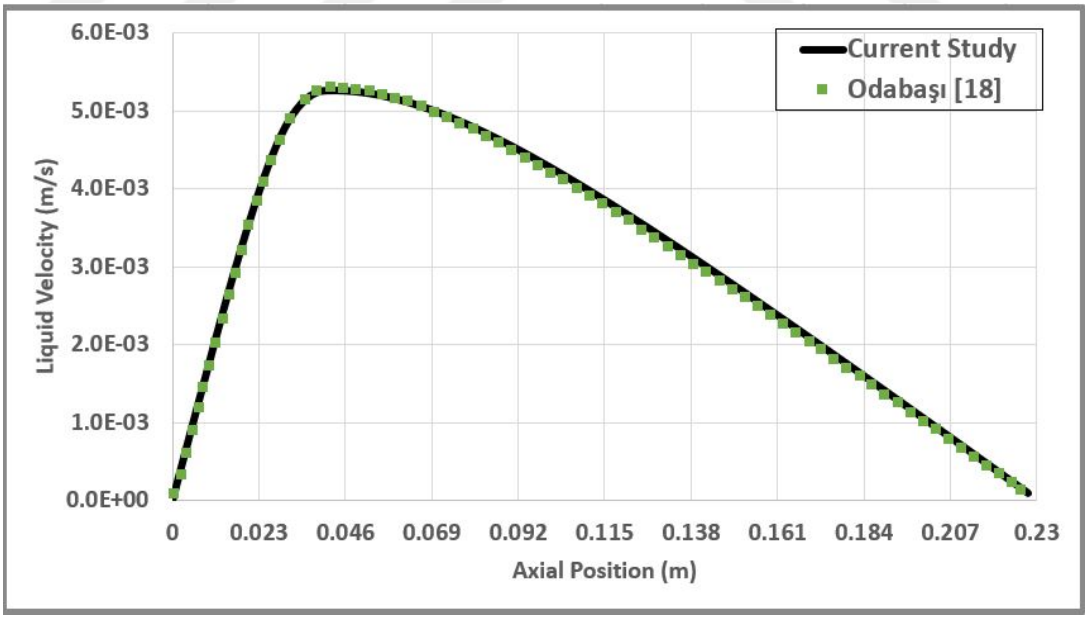

Figure 3.2: Liquid velocity

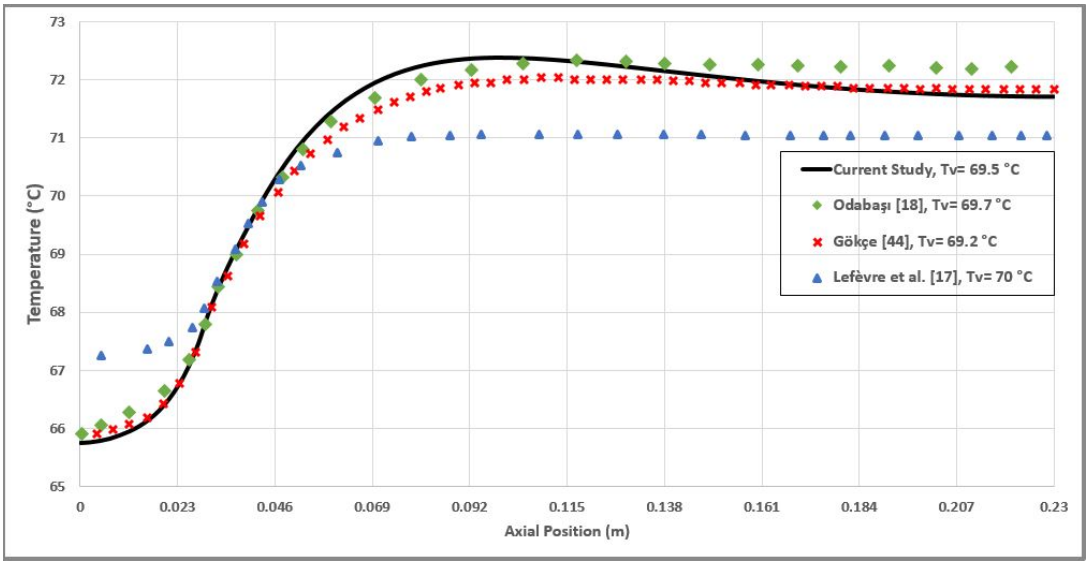

Figure 3.3: Wall temperature variation along heat pipe

al [29] did not applied special treatment for micro region heat transfer, they employed kinetic theory and used convective heat transfer coefficient for the entire liquid-vapor interface region.

In the current and Lefèvre et. al [29] thermal resistance analogy is used for thermal modeling. Different from these two studies, Odabaşı [30] utilized 3-D coordinate transformation for the heat transfer analysis. Whereas Gökçe [44] used a CFD based analysis methodology for the liquid flow and heat transfer.

Another validation study is carried out using the experimental and numerical results of Saygan [45]. Heat pipe having groove and fin width 600 μm and 400 μm fin height is simulated under different heat loads q=1.5 W/cm^2 and q=2.1 W/cm^2. Copper and isopropyl alcohol are used for the heat pipe material and working fluid, respectively. The length of the heat pipe is 100 mm with a evaporator and condenser 26 mm and adiabatic region 48 mm. Other material and geometrical properties are given in Table 3.2. Obtained wall temperature variations along the heat pipe are given in Fig. 3.4 and 3.5.

Table 3.2: Physical and geometrical properties used in the validation study

Length of FGHP (mm)	100
Half groove width, w_g (mm)	0.3
Half fin width, w_f (mm)	0.3
Base height, h_b (mm)	1.6
Fin height, h_f (mm)	0.4
Length of heat source region (mm)	26
Length of heat sink region (mm)	26

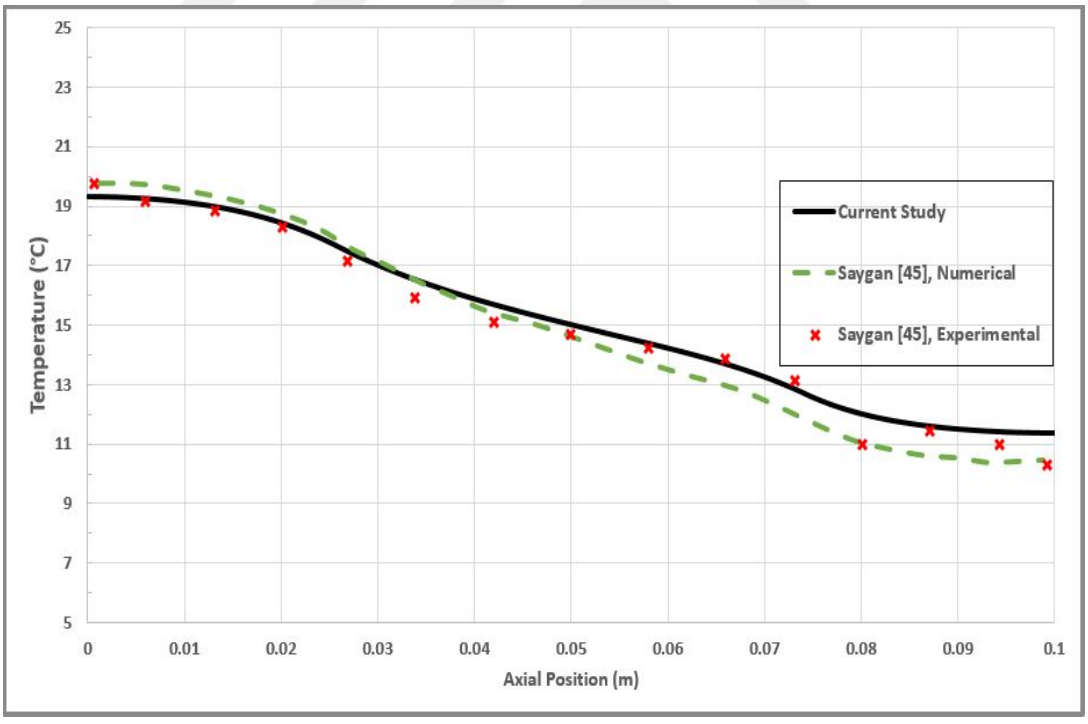

Figure 3.4: Wall temperature variation along heat pipe, *q"=1.5 W/cm²*

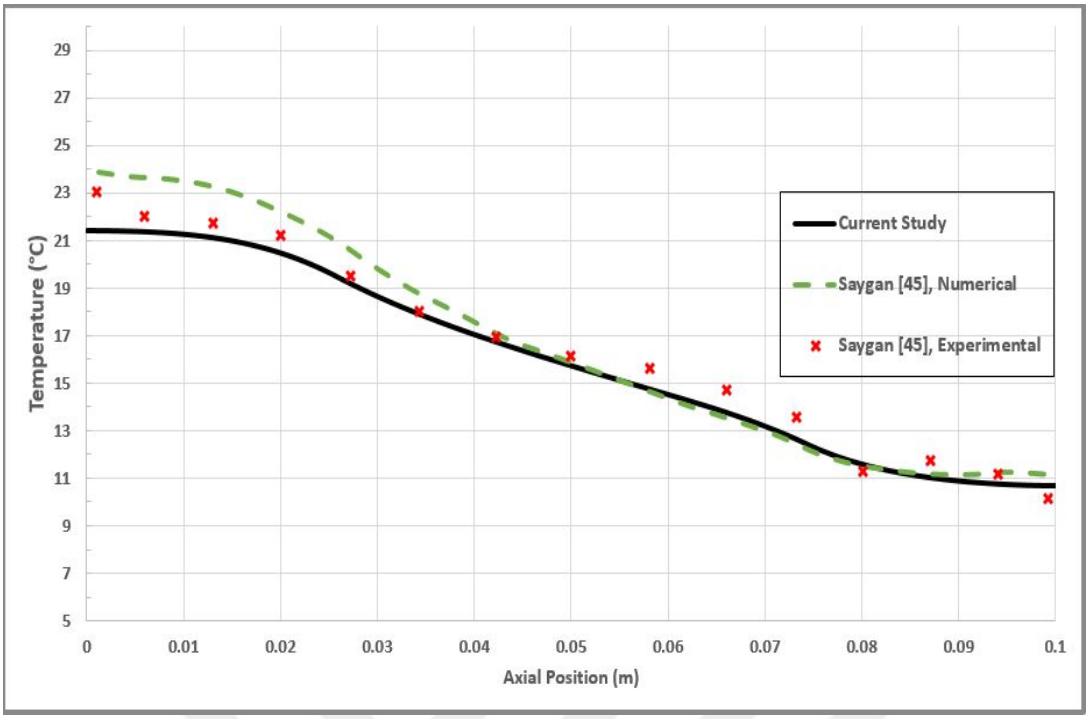

Figure 3.5: Wall temperature variation along heat pipe, q''=*2.1 W/cm*^{2}

In both studies, thermal resistance networks are used in order to simulate conducted heat transfer through the solid material and phase change heat transfer. In Saygan's study [45], micro and macro region evaporation and condensation introduced into thermal model with a set of resistances where in the current study, it is adapted into model with a single resistance for every control volume through the heat pipe. Despite using different approaches for phase change modeling, trends of the temperature variations show resemblance and good agreement with each other and the experimental results.

3.2 Validation Results for the Multi-channel Model

In this section experimental validation results of the developed multi-channel model are presented. An aluminum flat grooved heat pipe with a length 240 mm and isopropyl alcohol as working fluid are used in the experiments. In order to observed effect of the lateral heat transfer through the solid heat pipe material, local heat source and heat sinks not covering entire width of the flat grooved heat pipe are selected.

Heat source with length and width 27×12 mm and two heat sinks with length and width 20×50 mm are mounted.

To measure temperature values on several locations, 16 thermocouples are placed both through a center-line of heat pipe and through a line 20 mm offset from the center-line. 11 thermocouples are placed on centerline with 15 mm equally spaced and remainings are placed on off-center line with 30 mm equally spaced. Detailed view of the heat pipe used in the experiments is sketched in Fig. 3.6.

Table 3.3: Physical and geometrical properties used in the multi-channel validation study

Length of FGHP (mm)	240
Half groove width, w_g (mm)	0.25
Half fin width, w_f (mm)	0.25
Base height, h_b (mm)	1
Fin height, h_f (mm)	0.5
Length × width of heat source (mm)	27 × 12
Length × width of heat sink regions (mm)	20 × 50
Number of grooves	60
Heat load (W)	15

In Fig. 3.6, orange circles, red and blue rectangles represent the thremocouples, heater and heat sink regions, respectively. Black dashed lines stand for center-line and green dashed line indicates the off-center line. In the labeling of the thermocouples in Fig. 3.6, "TC-1S" means to symmetry of the "TC-1" with respect to vertical black dashed centerline.By taking the advantage of symmetry, only one-fourth of the entire FGHP is simulated using the multi-channel model.

In order to avoid the measurement errors, a reference temperature, T_{ref} is used. T_{ref} represents the average temperature of the 11 thermocouples placed on horizontal center-line. In the validation study, differences between the readings of the (TC-1

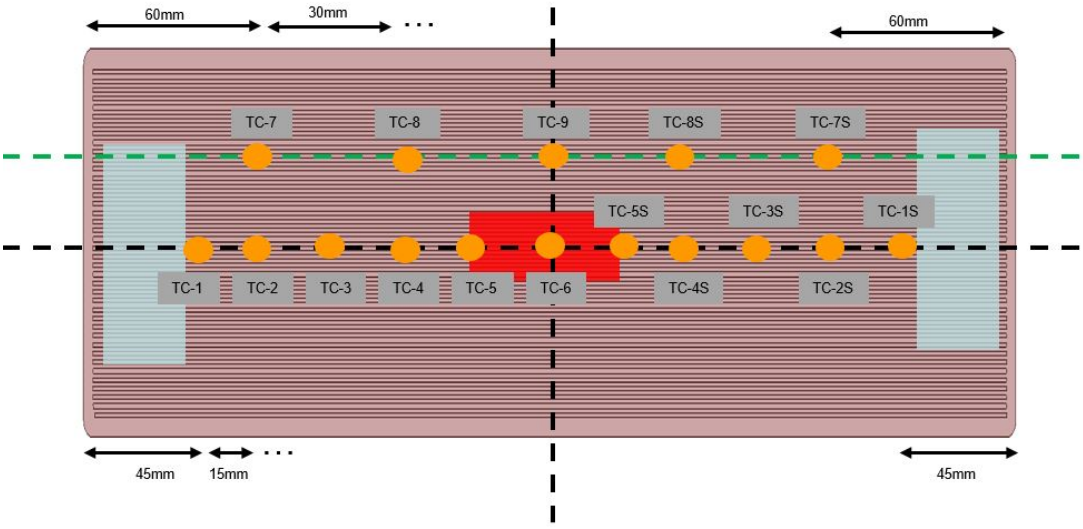

Figure 3.6: Detailed view of the flat grooved heat pipe with local heat source and heat sinks

- TC-9) and T_{ref} are taken as a basis.

$$\Delta T_{TC,i} = T_{TC,i} - T_{ref} \tag{3.1}$$

Measured differences obtained using the Eq. (3.1), compared with the calculated temperature differences between the corresponding nodes in multi-channel model and T_{ref}.

$$\Delta T_i = T_i - T_{ref} \tag{3.2}$$

Temperature difference variation through the FGHP is given Fig. 3.7. Maximum difference between the experimental and multi-channel model is calculated to be less than 1°C at TC-2 and TC-3. Calculated temperature difference variation trends shows well agreement with experimental results, especially in the off-center thermocouple readings, namely TC-7,8 and 9. This indicates that the developed multi-channel model is able to simulate effect of localized heat source and heat sink and to simulate conduction heat transfer between the neighbor grooves.

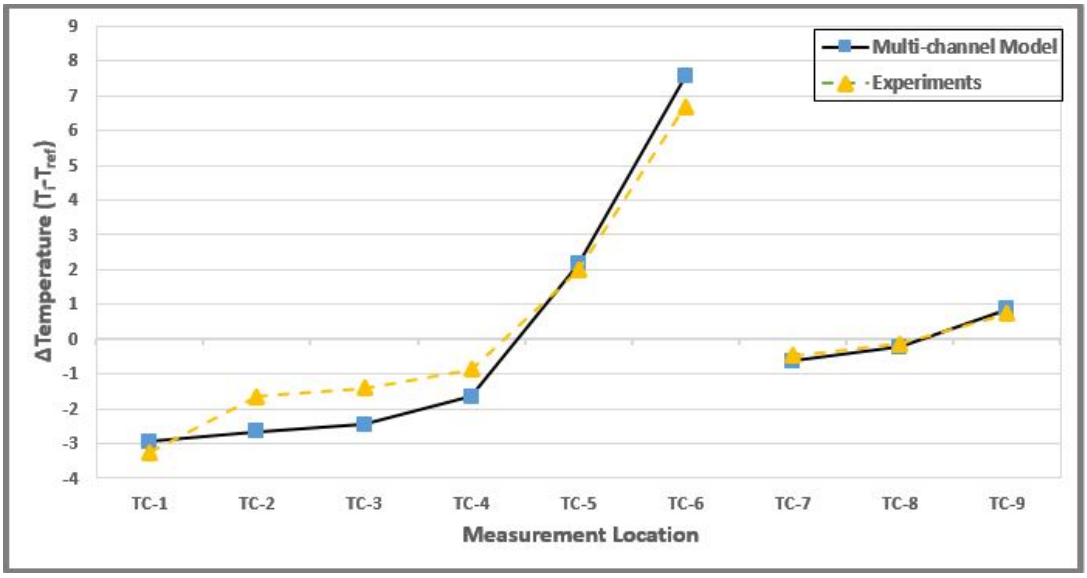

Figure 3.7: Temperature difference variation through FGHP

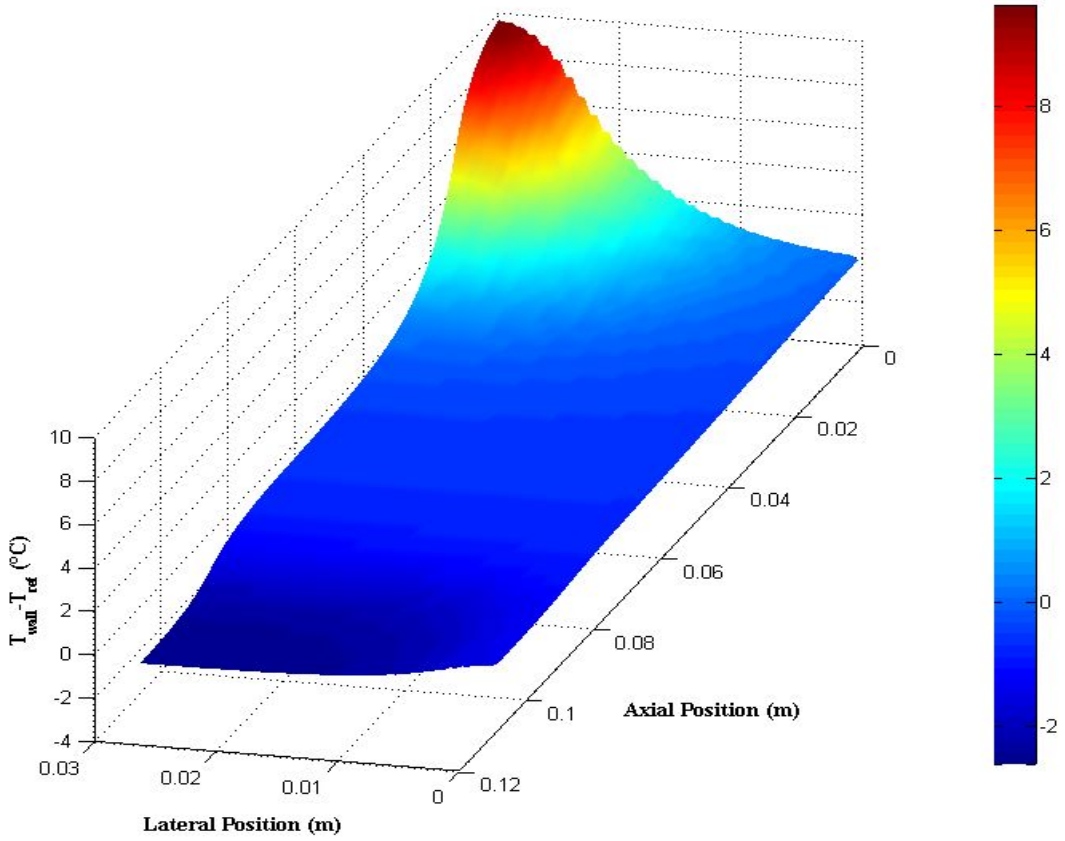

Figure 3.8: Temperature distribution through FGHP

CHAPTER 4

EXTENSION OF THE DEVELOPED MODELS TO COMPREHENSIVE PERFORMANCE ANALYSIS AND PARAMETRIC STUDY

In this chapter, developed half groove and multi-channel models are extended to be used in a comprehensive performance analysis and parametric study. In the first part of this chapter, multi-channel model is modified to observe the effect of the main frame surrounding the FGHP on the thermal performance. To do so, multi-channel resistance network is extended to capture the effect of the solid frame around the FGHP.

In order to understand the effect of groove and fin width variation for the same groove pitch value, a parametric performance analysis is performed. Temperature and contact angle differences between two ends of the heat pipe are used as the performance parameter for the better understanding the effect of the investigated parameters.

4.1 Extended Multi-channel Model and Effect of Solid Frame

Flat grooved heat pipe assemblies used in experimental studies basically consist of several parts like main frame, flat grooved heat pipe, covering frame, evaporator and condenser. Assembly of frame and FGHP are illustrated in Fig. 4.1. In the previous models explained in the Section 2.1.1 and 2.1.2, flat grooved heat pipe, evaporator and condenser are included in the models. In this section, effect of the main frame is taken into consideration and thermal resistance network of multi-channel model is extended in such a way that effect of the main frame can be observed. In order to reduce the effect of frame on the thermal of FGHP, materials have low thermal conductivity compare heat pipe base material are preferred to use. However, frames with

a cross-section larger than FGHP can affect the thermal performance and temperature distribution through FGHP. In Fig. 4.2, cross-section of a FGHP assembly is given. H_s and t are represented the height and thickness of the solid frame, respectively.

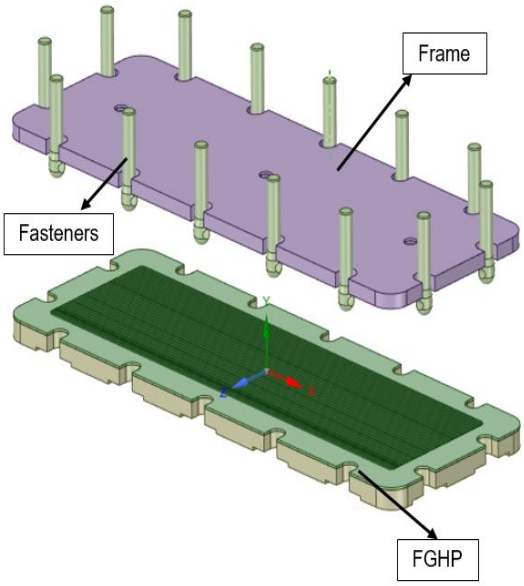

Figure 4.1: Main frame and flat grooved heat pipe

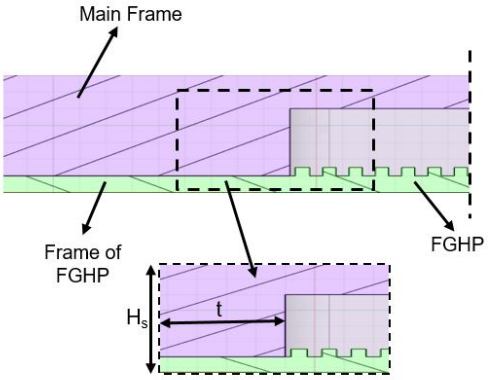

Figure 4.2: Cross-section of FGHP assembly

Thermal resistance network constructed for the multi-channel FGHP is extended such that effect of the frames can be represented. Thermal resistances are added so that heat conduction both in lateral and axial direction and natural convective heat transfer between the ambient and the frame can be regarded. Extended thermal resistance

network is presented in Fig. 4.3.

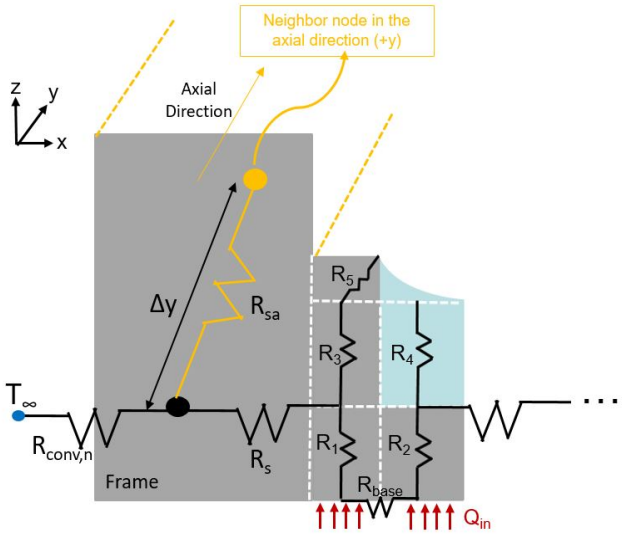

Figure 4.3: Extended thermal resistance network with frame structure

Resistance, R_{sa} is stand for the heat conduction through the solid frame in the direction of $(+y)$. In addition, node colored with orange represented the neighbor thermal node of the solid frame in the axial direction $(+y)$. R_s and $R_{conv,n}$ are the thermal resistances for heat conduction in lateral directiond and natural convection,respectively. Expressions for the added thermal resistances are given in Eq. (4.1-4.3) where h_n is the natural convection heat transfer coefficient.

$$R_s = \frac{w_f/2 + t/2}{k_s(h_f + h_b)\Delta y} \tag{4.1}$$

$$R_{sa} = \frac{\Delta y}{k_s t H_s} \tag{4.2}$$

$$R_{conv,n} = \frac{1}{h_n H_s \Delta y} \tag{4.3}$$

The effect of the solid frame is investigated with a study which has a physical and geometrical properties as provided in Table 4.1.

In addition to properties given Table 4.1, solid frame material is also a crucial param-

Table 4.1: Physical and geometrical properties used in the investigation of frame effect

Length of FGHP (mm)	120
Half groove width, w_g (mm)	0.25
Half fin width, w_f (mm)	0.25
Base height, h_b (mm)	1
Fin height, h_f (mm)	0.5
Length of heat source region (mm)	30
Length of heat sink region (mm)	30
Heat load (W/cm^2)	4
Ambient temperature (°C)	10
Thickness of the frame,t (mm)	15
Height of the frame,H_s (mm)	12
Number of grooves	24

eter for better understanding the effect of the solid frame on the thermal behaviour of the FGHP. Therefore, three different performance analysis studies are conducted of the same configuration without a frame structure and with a stainless steel frame structure. Evaporator and condenser region of the FGHP are illustrated in Fig. 4.4. Thermal resistance network of the system is constructed only for one-fourth of the FGHP due to the symmetry.

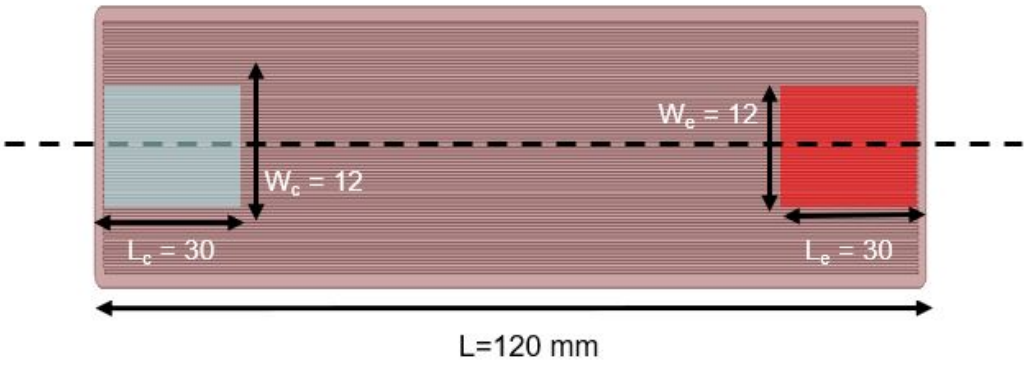

Figure 4.4: Evaporator and condenser region of the FGHP

First, results of the simulation not included the frame structure is given. Temperature distribution of the interested region is provided in Fig. 4.5.

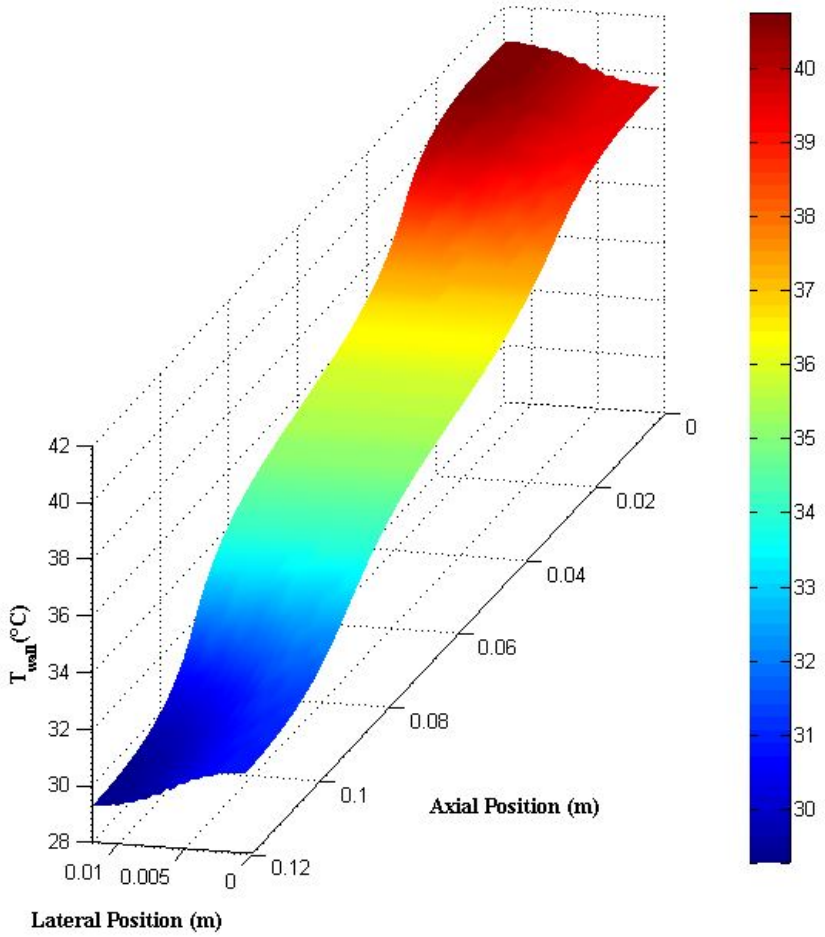

Figure 4.5: Temperature distribution through FGHP without a frame structure

Vapor temperature is calculated as 35.5°C. Since the lateral heat conduction is taken into account and local evaporator and condenser regions are involved, temperature difference between the two ends varies along the lateral direction. While maximum temperature difference between the ends is observed as 11.5°C along the dashed line given in Fig. 4.4, minimum temperature difference is monitored as 8.6°C in the outermost groove from the dashed centerline. In addition, maximum temperature calculated as 40.8°C.

In order to spot the effect of the frame structure on the thermal performance, operation of the FGHP having a frame made of stainless is simulated under the conditions

given in Table 4.1. Temperature variation through FGHP is shown in the Fig. 4.6 With a stainless steel frame, vapor temperature of the FGHP is predicted as 34.3°C. Maximum temperature difference between the two ends is similar to case without frame structure and calculated as 11.2°C. Also, observed minimum temprature difference between the evaporator and condenser end is comparable with the frameless case with value 8.2°C. As a result of the convective heat transfer with the ambient, highest temperature is observed as 39.4°C.

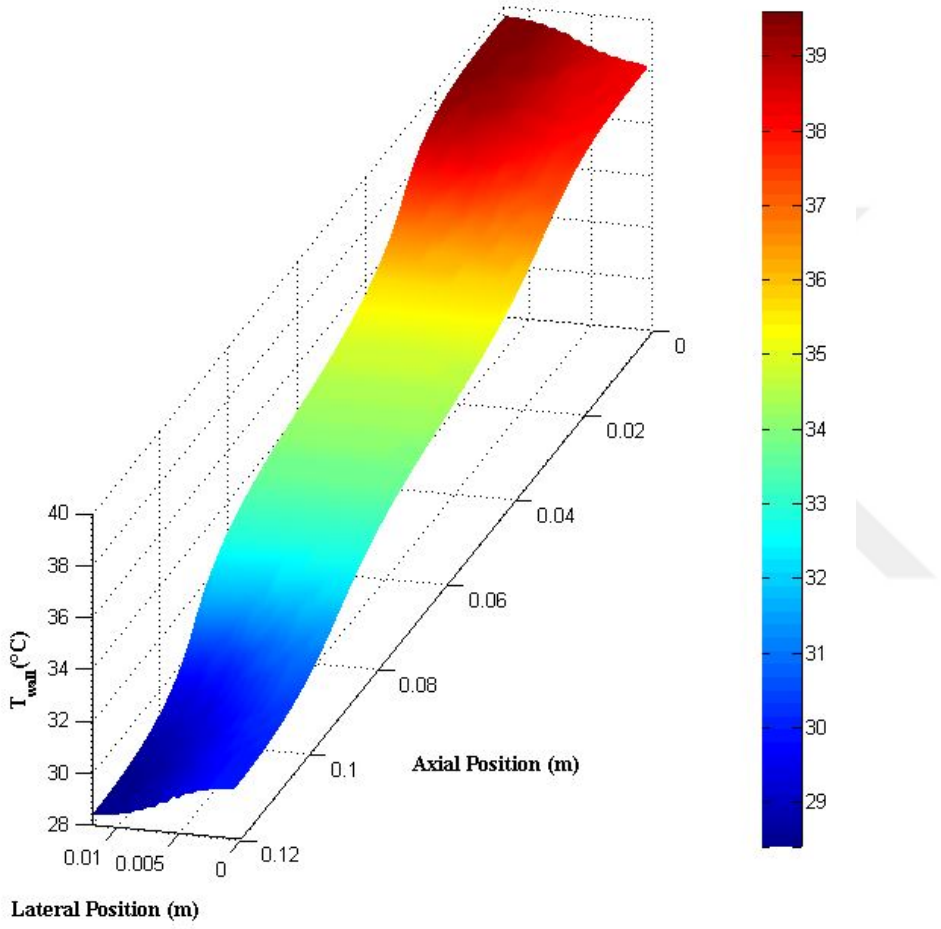

Figure 4.6: Temperature distribution through FGHP with a stainless steel frame

4.1.1 The Effect of the Solid Frame Material

In this section, to show the effect of the solid frame material selection, performance analysis study is repeated with copper frame instead of stainless steel. Stainless steel and copper are selected for the comparison study due the differences in their thermal

conductivities. Stainless steel has a thermal conductivity about 16 W/mK, whereas copper's thermal conductivity is about 400 W/mK. In this simulation, same configuration and properties provided in Table 4.1 and Fig. 4.4 are used.

Temperature variation through the FGHP can be seen in Fig. 4.7. Due the high thermal conductivity of the frame, in the grooves close to the frame region (half groove number-1 in Fig. 4.7 is the nearest), heat is conducted through the frame in addition to the phase change heat transfer and conduction heat transfer through heat pipe's solid material.

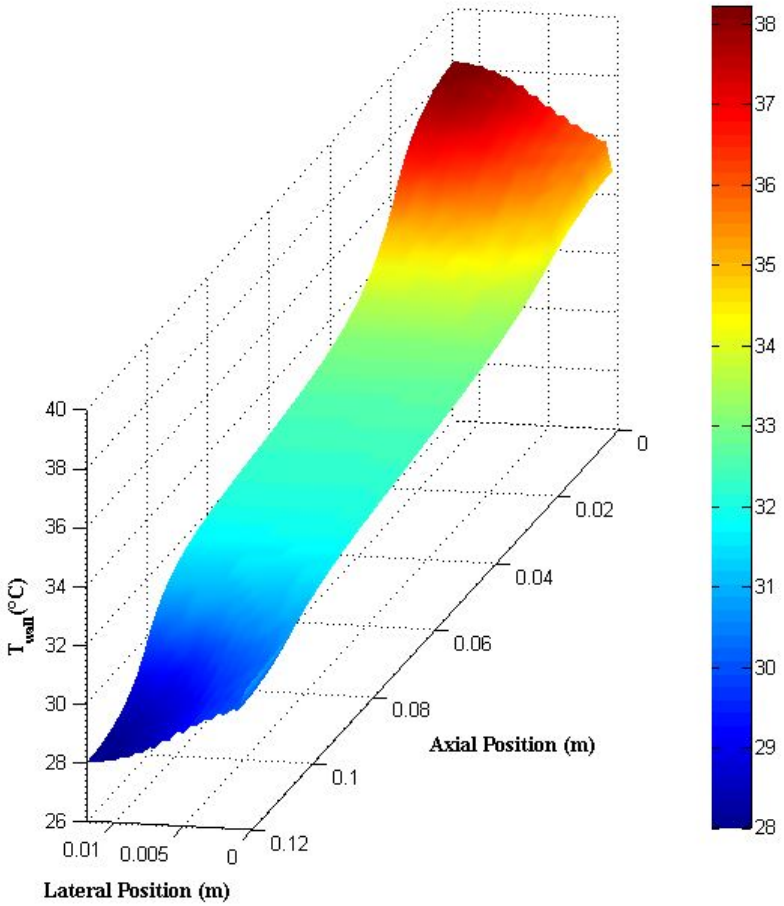

Figure 4.7: Temperature distribution through FGHP with a copper frame

Vapor temperature during the operation is calculated as 33.1°C. Maximum and minimum temperature differences between the evaporator and condenser end of the FGHP are 10.6°C and 4.4°C. Wall temperature variation along the nearest groove to the frame (farthest groove from the centered dashed line in Fig. 4.4) is given Fig. 4.8.

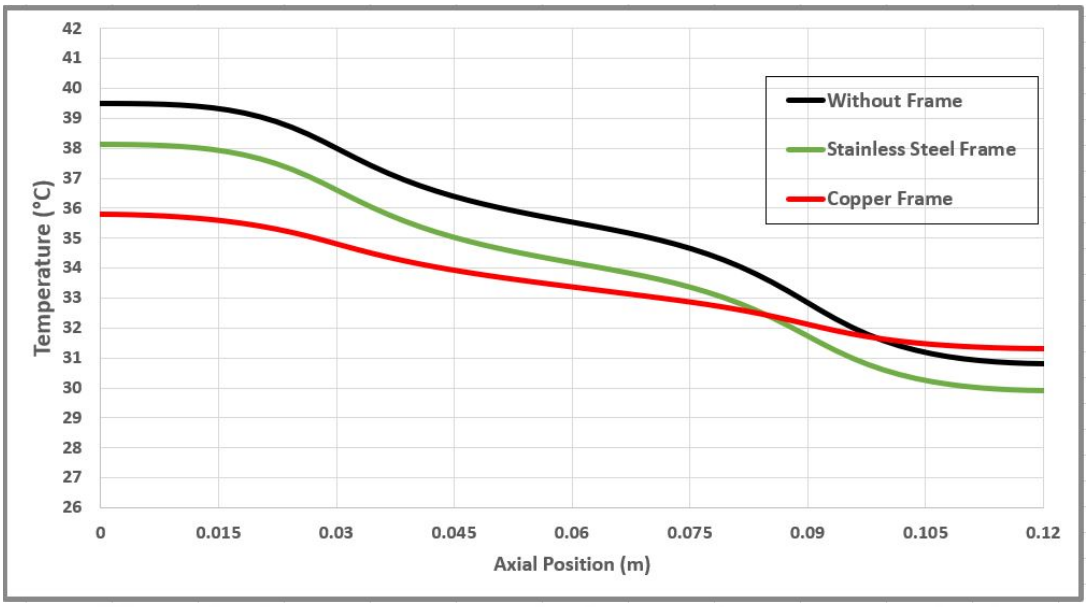

Figure 4.8: Temperature variation along nearest groove to the frame structure

As seen in the provided results, using a frame having higher thermal conductivity resulted in more uniform temperature distribution near the frame structure and lower working temperature. In order to conduct a detailed performance analysis for FHGP and predict working parameters correctly effect of frame the should be taken into consideration especially FHGP with frame structure having comparable thermal conductivity with heat pipe base material.

4.1.2 The Effect of the Solid Frame for Different Groove Numbers

In this section the effect of the solid frame is investigated for different number of grooves. Flat grooved heat pipe with a copper frame is used for the analysis. All physical and geometrical properties are kept identical as in Section 4.1 except number of grooves and width of heating and cooling areas. All properties are given in Table 4.2. Heat source and heat sink are considered such that they cover entire width of the heat pipe. Location of the evaporation and condensation regions are illustrated in Fig. 4.9.

Table 4.2: Physical and geometrical properties used in the investigation of the effect of groove number with frame structure

Length of FGHP (mm)	120
Half groove width, w_g (mm)	0.25
Half fin width, w_f (mm)	0.25
Base height, h_b (mm)	1
Fin height, h_f (mm)	0.5
Length of heat source region (mm)	30
Length of heat sink region (mm)	30
Heat load (W/cm^2)	1.8
Ambient temperature (°C)	10
Thickness of the frame,t (mm)	15
Height of the frame,H_s (mm)	12

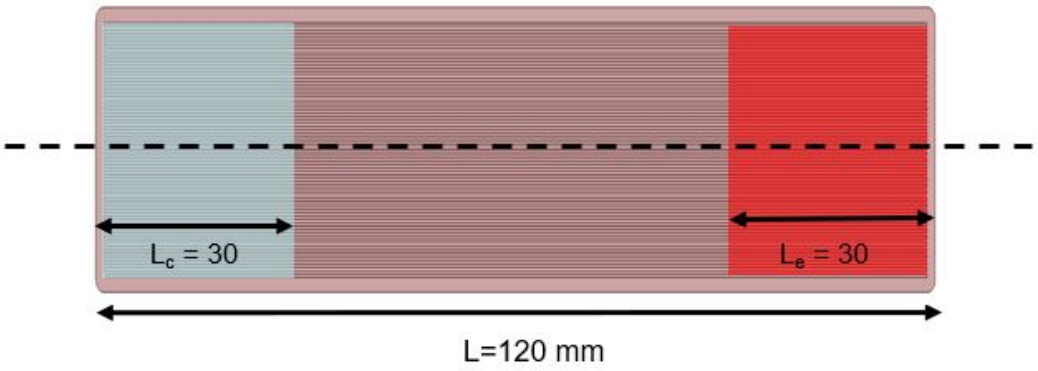

Figure 4.9: Evaporator and condenser region of the FGHP

Performance analysis of FGHP's having 1, 4, 8, 12, 24 and 32 grooves are conducted. Benefiting from the symmetry, only the half of FGHP's are modeled. Temperature surface plots through out the FGHP's are given in Fig. 4.10-4.12.

Thermal resistance due to the frame structure become more remarkable on overall thermal resistance with decreasing number of grooves. Therefore effect of solid frame on temperature distribution is decreasing with increasing number of grooves

as expected. The ratios of phase change heat transfer to the total heat load are 7%, 15%, 29%, 40%, 63% and 72% for the FGHP's having 1, 4, 8, 12, 24 and 32 grooves, respectively. On the other hand, the ratio of phase change heat transfer to the total heat load for the model without frame structure is calculated as 93%.

Around the evaporator end of heat pipe, grooves close the frame structure have lower temperature values compare to grooves far away from the frame. On the contrary, around the condenser end, grooves close the frame structure have higher temperature compare to grooves far away from frame as a result of the heat conduction through the solid frame. The variation of the wall temperature along the nearest groove to the frame (farthest groove from the centered dashed line in Fig. 4.9) and along the farthest groove from the frame (nearest groove to the centered dashed line in Fig. 4.9) are given in Fig. 4.13 and 4.14, respectively.

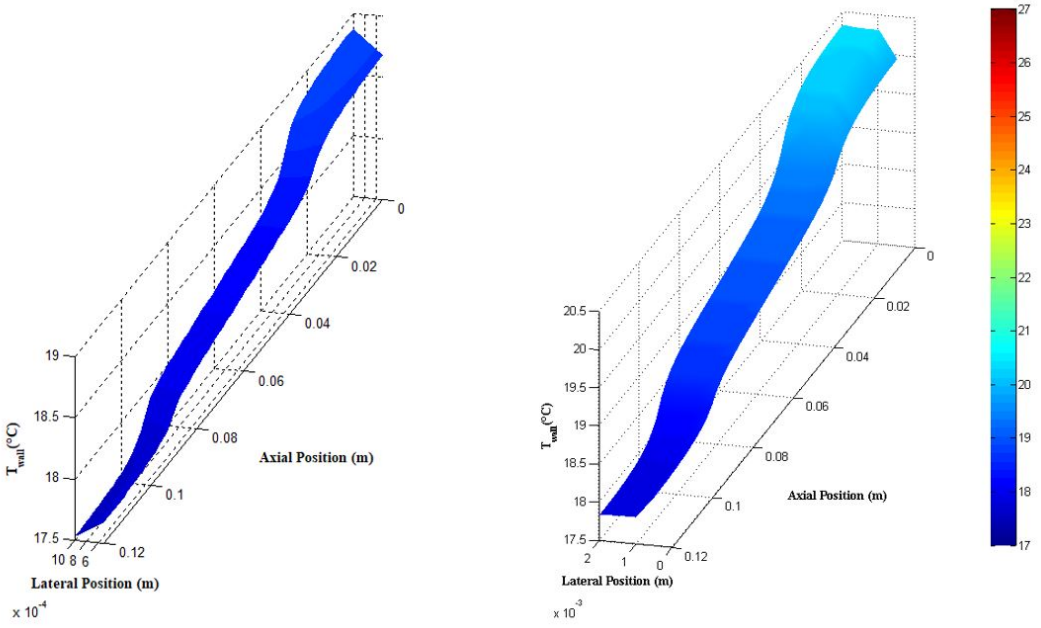

Figure 4.10: Temperature distributions through FGHP having 1 groove and 4 grooves

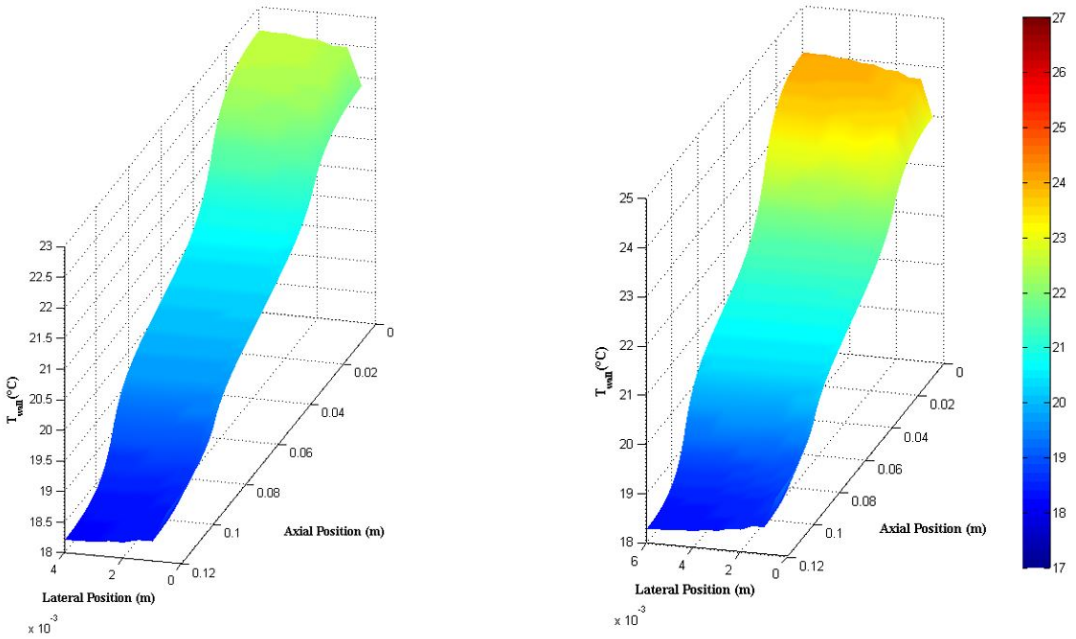

Figure 4.11: Temperature distributions through FGHP having 8 and 12 grooves

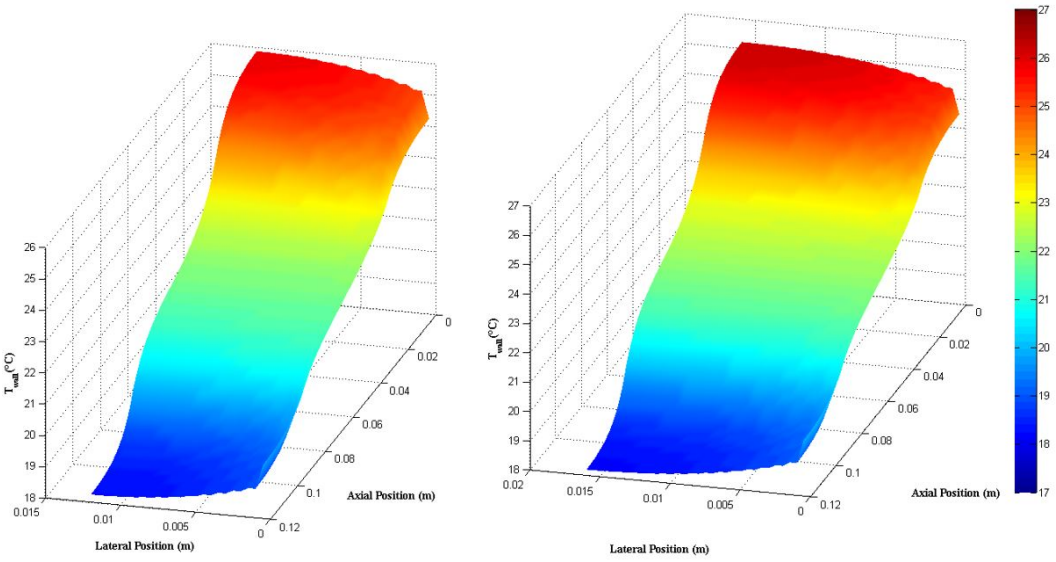

Figure 4.12: Temperature distributions through FGHP having 24 and 32 grooves

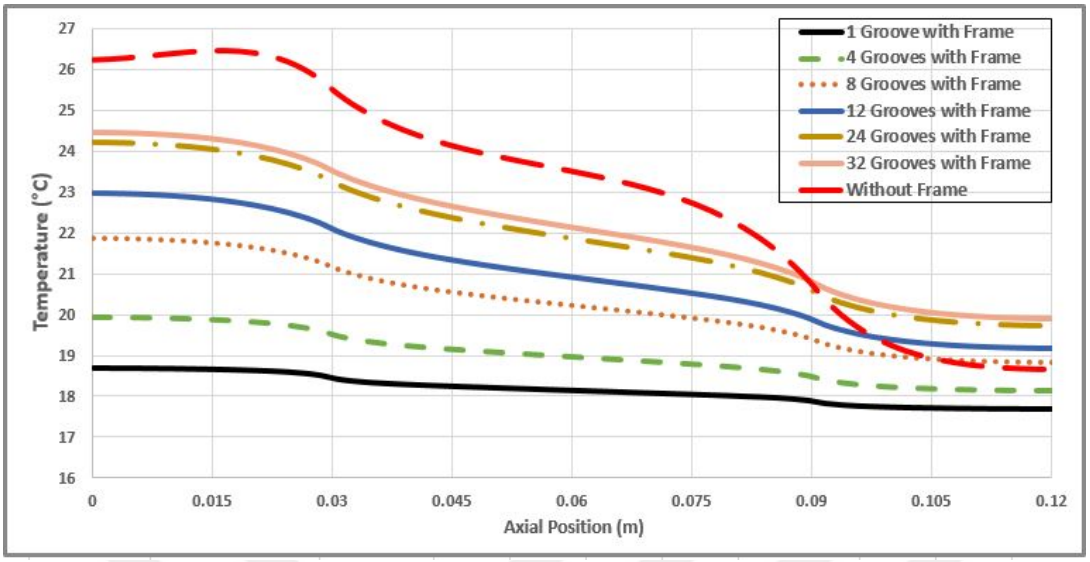

Figure 4.13: Temperature variation along the nearest groove to the frame for different number of grooves

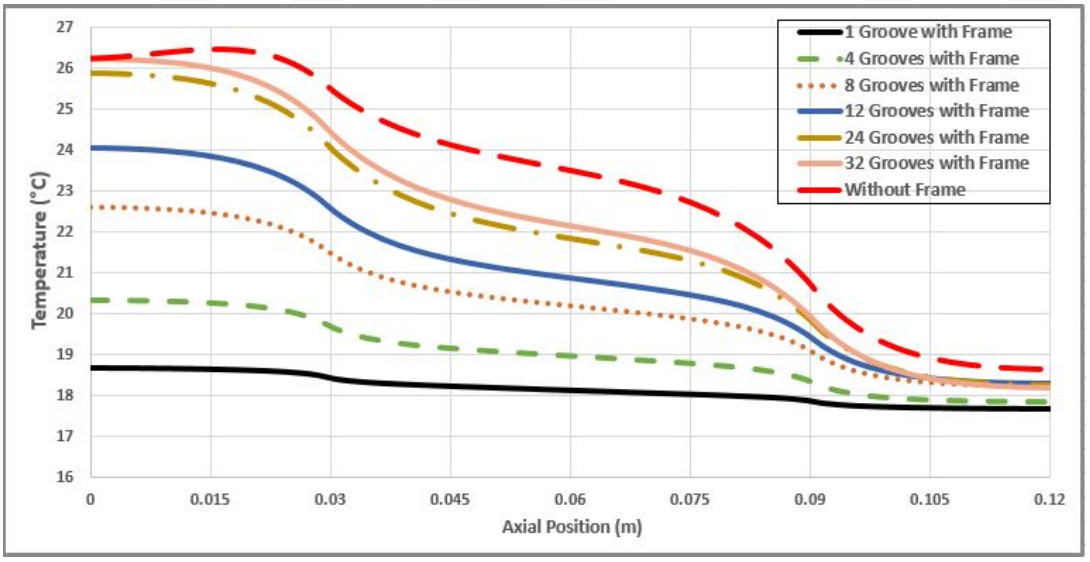

Figure 4.14: Temperature variation along the farthest groove from the frame for different number of grooves

4.2 The Effect of Localized Heating on Thermal Performance

In this section, solid frame extended multi-channel is used to observe the effect of localized heat source on the thermal performance of FGHP. Under a localized heating and cooling conditions, performance of FGHP is monitored and maximum heat transfer capacity before dry-out limit is determined. Then, by using the half groove model, dry-out limit of same configuration is determined under a entirely covering heater instead of localized heating. Physical and geometrical properties used in the study are given in Table 4.3. In addition to properties in Table 4.3, working fluid and solid base material is selected isopropyl alcohol and copper, respectively. Location of the localized heating and cooling region are illustrated in Fig. 4.15.

Table 4.3: Physical and geometrical properties used in the multi-channel validation study

Length of FGHP (mm)	120
Half groove width, w_g (mm)	0.25
Half fin width, w_f (mm)	0.25
Base height, h_b (mm)	1
Fin height, h_f (mm)	0.5
Length $\times$ width of heat source (mm)	13.5 $\times$ 20
Length $\times$ width of heat sink regions (mm)	10 $\times$ 50
Number of grooves	60
Ambient temperature (°C)	0
Thickness of the frame,t (mm)	15
Height of the frame,H_s (mm)	12

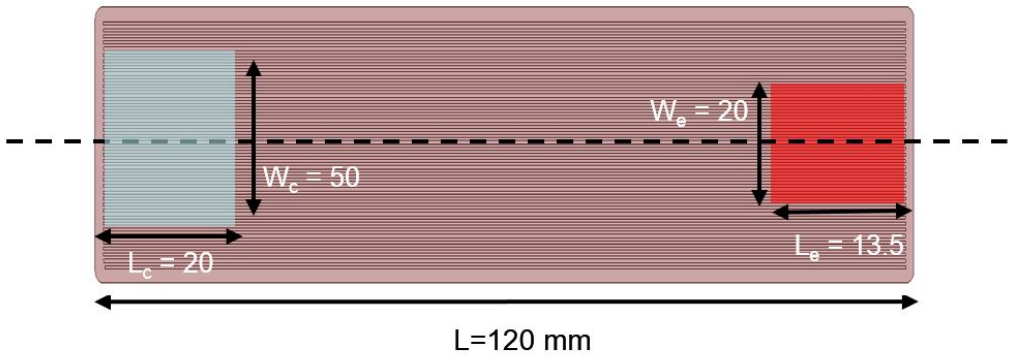

Figure 4.15: Evaporator and condenser region of FGHP

By using the symmetry, half of the FGHP is modeled. Heat flux 6.5, 7.5, 8.0 and 8.2 W/cm^2 are applied as a heat load from the corresponding heating areas for four different simulations. Temperature surface plots through FGHP's under different heat fluxes are given in Fig. 4.16–4.17.

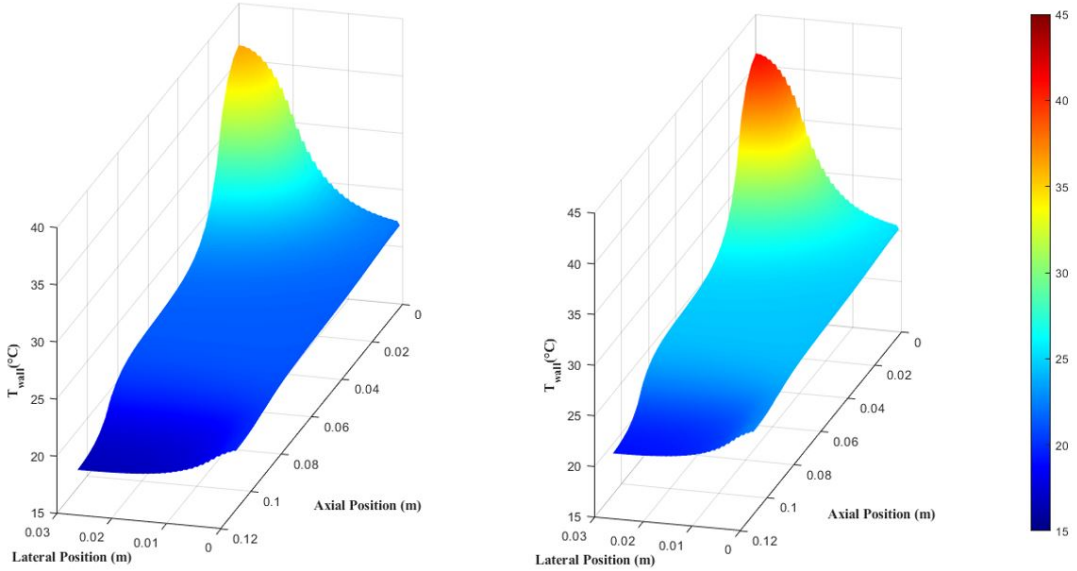

Figure 4.16: Temperature distributions through FGHP, $q^{''} = 6.5$ and $q^{''} = 7.5$ W/cm^2

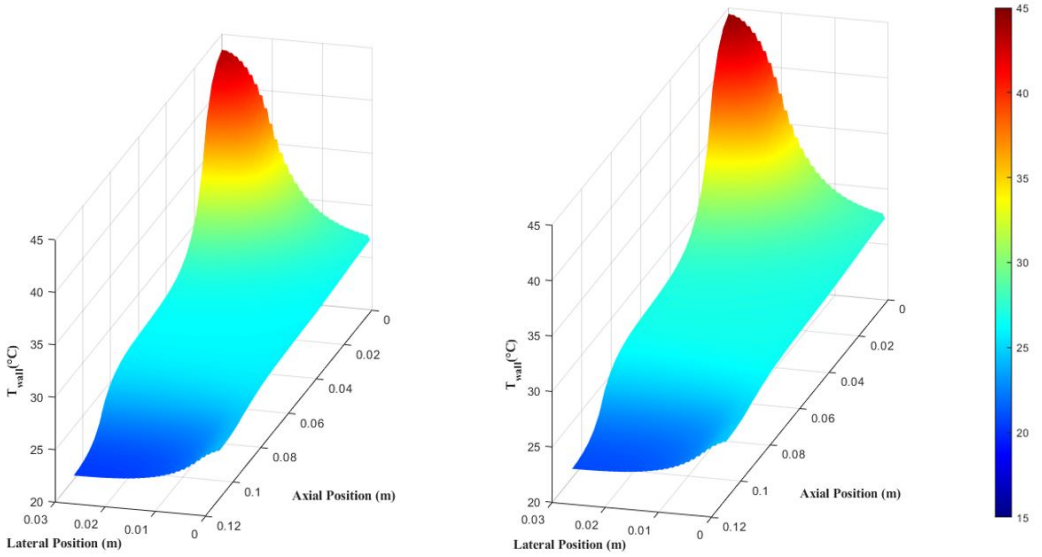

Figure 4.17: Temperature distributions through FGHP, $q^{''} = 8.0$ and $q^{''} = 8.2$ W/cm^2

When the heat load $q^{''} = 8.2$ W/cm^2 is applied, contact angle at the end of the evaporator region regions its minimum value which is called material contact angle. Further increasing in the heat load will result in dry-out at the evaporator region. Therefore, for this localized heating and cooling configuration maximum heat load capacity of the FGHP is calculated $q^{''} = 8.2$ W/cm^2 ($q = 22.1$ W).

Similar simulation are repeated by neglecting the frame and localized heating and cooling effects until maximum heat load capacity of FGHP is reached which is $q^{''} = 3$ W/cm^2 ($q = 24.3$ W). Temperature distribution for this case is given in Fig. 4.18.

FGHP having localized heat source and heat sink is capable of transport $q = 22.1$ W before dry-out limit was reached. On the other hand, FGHP with a heat source entirely covering the width is capable of transport $q = 24.3$ W heat input. As a result, localizing heat source and heat sink, resulted in a decreasing in maximum heat load capacity of FGHP. In addition, localized heat source bring hot spot region on the FGHP. While maximum calculated temperature with a entirely spreaded heat source is $35.1°$C, it is $44.4°$C with a localized heat source before dry-out limitations of the same configuration.

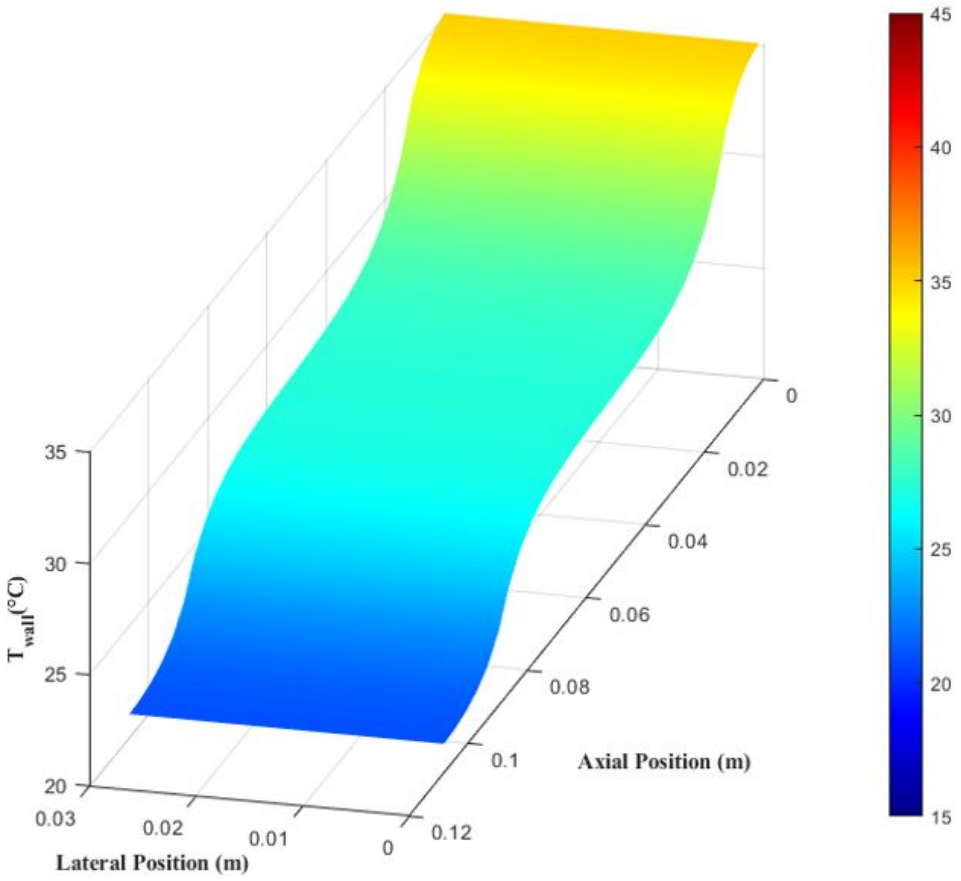

Figure 4.18: Temperature distributions through FGHP by neglecting frame and localized heating and cooling

4.3 The Effect of Groove and Fin Width for Constant Groove Pitch

In this section, performance effect of the different groove-fin width ratios for a constant groove pitch is investigated. Groove pitch can be defined as the total width of a half groove and a half fin widths.

In this parametric study, isopropyl alcohol and copper are selected as the working fluid and solid base material, respectively. Performance analyzes are conducted by using the half-groove thermal resistance model. Some geometrical groove dimensions and parameters are given Table 4.4.

Through out this study, various groove-fin width ratios for different groove pitches are studied. Parametric simulations are conducted for groove pitches and groove-fin

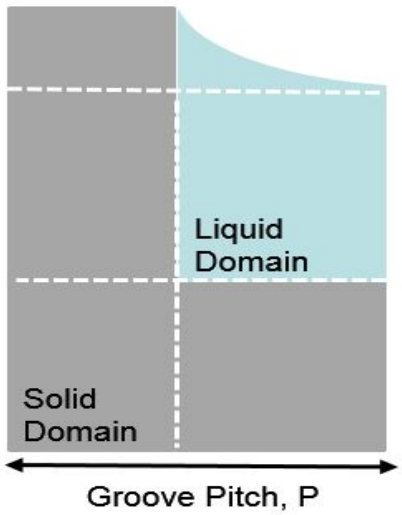

Figure 4.19: Groove pitch

Table 4.4: Physical and geometrical properties used in the parametric study

Length of FGHP (mm)	100
Base height, h_b (mm)	1.6
Fin height, h_f (mm)	0.4
Length of heat source region (mm)	26
Length of heat sink region (mm)	26
Heat transfer coefficient (W/m^{2}K)	1000
Heat load (W/cm^2)	1.5
Ambient temperature ($^\circ$C)	10

widths provided in Table 4.5. All dimensions are given in micrometers.

For the physical and geometrical properties given in Table 4.4, solutions of the some groove-fin width ratios can not be obtained due to the falling of contact angle till the limits of material contact angle for working fluid and base material. Therefore, simulations that dry-out occurred are not used in the parametric study. For all groove pitch values, narrower groove widths without dry-out are included in the study and domain of the parametric study is updated as in Table 4.6.

Temperature difference between two ends of the heat pipe is given in Fig. 4.20 for

Table 4.5: Groove and fin widths for different groove pitches

GROOVE PITCH							
600		**400**		**200**		**100**	
Groove Width	**Fin Width**	**Groove Width**	**Fin Width**	**Groove Width**	**Fin Width**	**Groove Width**	**Fin Width**
150	1050	100	700	50	350	25	175
300	900	200	600	100	300	50	150
450	750	300	500	150	250	75	125
600	600	400	400	200	200	100	100
750	450	500	300	250	150	125	75
900	300	600	200	300	100	150	50
150	1050	700	100	350	50	175	25

Table 4.6: Groove and fin widths for different groove pitches without dry-out limitations

GROOVE PITCH							
600		**400**		**200**		**100**	
Groove Width	**Fin Width**	**Groove Width**	**Fin Width**	**Groove Width**	**Fin Width**	**Groove Width**	**Fin Width**
-	-	-	-	-	-	-	-
400	800	-	-	-	-	-	-
450	750	320	480	-	-	-	-
600	600	400	400	220	180	-	-
750	450	500	300	250	150	140	60
900	300	600	200	300	100	150	50
150	1050	700	100	350	50	175	25

several dimensionless groove widths where dimensionless groove width is defined as the ratio of the groove width to the groove pitch. As seen in the Fig. 4.20, for the same dimensionless groove width, temperature differences are decreasing with decreasing groove pitch and heat pipes show better performance for the under the same conditions. This performance enhancement is observed as a result of thinner film thicknesses both in fin top region at the condenser and the evaporation region. Thinner film thicknesses lead to lower thermal resistances and the same heat load is transferred with lower temperature differences.

In a similar manner, with the decreasing groove width, heat pipes are getting able to transfer same amount of heat with low temperature differences for the same groove pitch as a result of thinner film thickness.

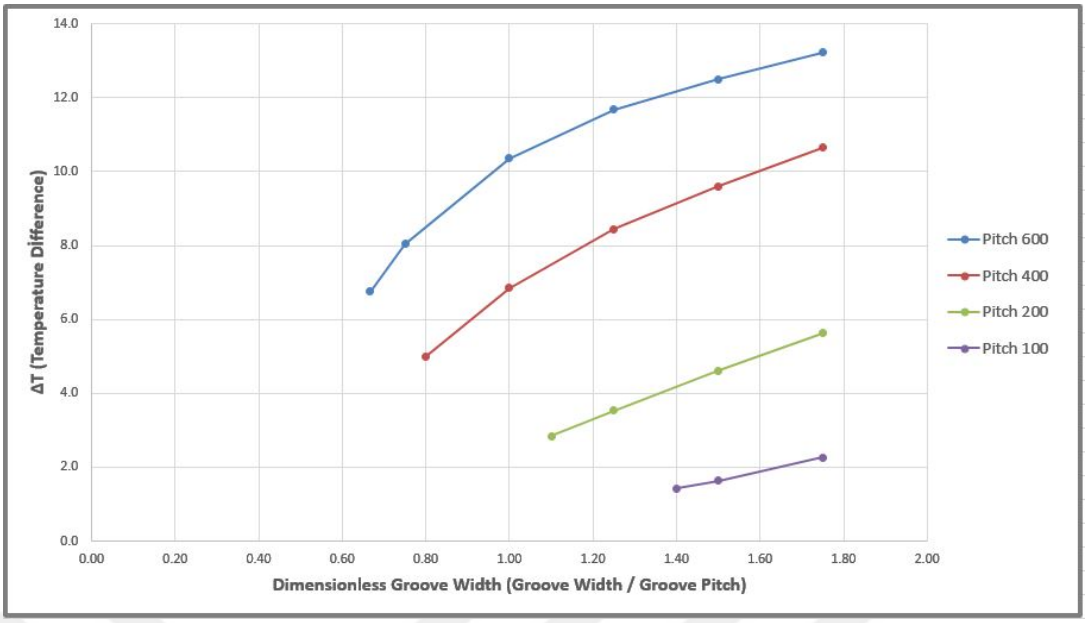

Figure 4.20: Temperature difference variations for different groove pitches

Another important parameter examined during the parametric study is contact angle difference between two ends of the heat pipe. Contact angle variation along the heat pipe creates the necessary driving force for the fluid flow. Contact angle difference between two ends of the heat pipe is given in Fig. 4.21 for the dimensions given in Table 4.6.

In Fig. 4.21, for the same dimensionless groove width, contact angle differences are increasing with the decreasing groove pitch. When Fig. 4.20 and 4.21 are evaluated together, it is concluded that for all groove pitches while temperature differences are decreasing, required contact angle differences to drive working fluid are increasing. For the same groove pitch, heat pipes with lower contact angle differences can transfer higher amount heat without dry-out. Although lower temperature differences are observed in heat pipes having narrow groove widths, dry-out phenomena will take place in lower heat inputs compare to heat pipes having wider groove widths. Therefore, geometrical dimensions and groove-fin width ratio of a heat pipe should be selected properly by considering the application it will be used.

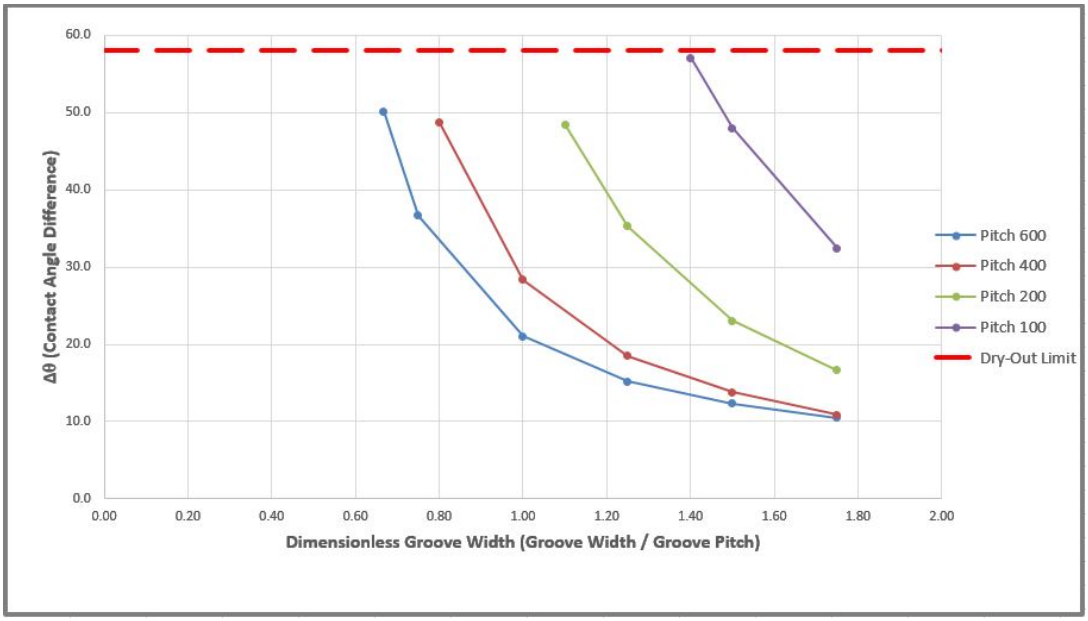

Figure 4.21: Contact angle difference variations for different groove pitches

CHAPTER 5

CONCLUSION AND SUGGESTIONS FOR FUTURE WORK

Heat pipes have been widely used in thermal management of various applications owing to their ability to transfer high amounts of heats with temperature gradients. Although there are several studies conducted to understand physics behind the heat pipes, modeling of heat pipes are still a challenging task due to it complicated and coupled nature.

In this thesis study, developing fast and accurate flow and heat transfer models able to calculate several working parameters of heat pipe is aimed. First, benefiting from the symmetry, thermal resistance analogy based half-grooved model is developed. Beside heat transfer modeling, evaporation and condensation phase change models have significant importance on the accurate predictions of thermal performance. Therefore, by employing the kinetic theory, detailed mathematical models are generated. Since it is essential to validate suggested models, both experimental and numerical results provided in the literature for flow and heat transfer models are used.

In real life applications, it is not always the case to exposure symmetrical heating and cooling. Therefore, the need of developing 3D thermal resistance network enables to apply local heating and cooling is arises in order to predict the performance of heat pipe precisely. Developed and validated half groove model extended to a multi-channel heat transfer model. In multi-channel model, in addition to connecting neighbor grooves, external grooves are connected to frame structure to take into consideration heat conduction through solid frame. Validation study of the suggested multi-channel model is conducted using results of experimental setup having localized heat source and sink. Using the temperature readings from both center and off-center lines through the heat pipe, capability of capturing different temperature

variation trends in the center and off-center lines of the developed model is shown.

In the parametric studies, effect of several physical and geometrical parameters are investigated. Effect of solid frame for different point views are investigated. First, performance analysis are conducted for different solid frame materials. The obtained temperature distributions show that using a frame having higher thermal conductivity resulted in more uniform temperature distribution near the frame structure and lower working temperature for the heat pipe. Near the frame structure, temperature difference between the two ends of the heat pipe is calculated as 8.2°C in the case of stainless steel frame. Whereas, the difference between the same locations is about 4°C.

Another parametric study is conducted to investigate the significance of solid frame effect for the heat pipes having different number of grooves. By calculating the ratios of phase change heat transfer to the total heat load, it is concluded that contribution of the solid frame to the overall heat transfer is decreasing with increasing number of grooves. The ratios are obtained as 7%, 15%, 29%, 40%, 63% and 72% for the FGHP's having 1, 4, 8, 12, 24 and 32 grooves, respectively. For narrower heat pipes, a significant portion of the heat transferred by conduction through the solid frame structure and it is decreasing while heat pipe is getting wider (with increasing number of grooves).

An important phenomena for an operation heat pipe called dry-out is investigated under a localized heat source and sink. Performance of FGHP under a localized heating and cooling conditions is monitored and heat load is increased until the maximum heat transport capacity is reached. Obtained results for locally heated FGHP are compared with a model having heat source covers entire width instead a localized one. It is shown that while having a localized heat source, FGHP is able to transport $q = 22.1$ W heat before dry-out limit was reached. On the other hand, FGHP with a heat source entirely covering the width is capable of transport $q = 24.3$ W heat input. The findings of the conducted study indicate the importance of taking into consideration localized heating and cooling effects while dealing with the dry-out phenomena of an operating heat pipe.

In the last part of the parametric study, performance effect different groove-fin width

ratios is investigated. Temperature differences and contact angle variations are compared for the different width ratios. From temperature difference point of view, FGHP having narrower grooves show better thermal performance since they are able to transfer same amount of heat with lower temperature difference compared to FGHP having wider grooves. However, required contact angle difference to drive the working fluid is increasing while groove of the FGHP is getting narrower. As a result of the study, it is concluded that although dry-out phenomena takes places with lower heat inputs, heat pipes having narrow grooves are able transfer same amount of heat with lower temperature differences. Design of the grooves should be determined and optimized according the particular requirements of the thermal system.

To sum up, in current thesis study, mathematical models are developed and verified. Then, validated models are used to investigate different performance parameters under various physical and geometrical conditions. As an extension of this thesis study, following topics can be recommended for the future studies:

- Performance analysis of the heat pipes have rectangular grooves are conducted for both half-groove and multi-channel geometries. Constructed thermal resistance networks can be modified such that the effect of different groove shapes and geometries are observed.
- When the dry-out phenomena are considered, it is only determined whether dry-out takes place or not with the current model by controlling the contact angles at the evaporator end of the heat pipe. Performance effect of the dry-out can be implemented to the developed model for the more detailed performance analysis.
- Similar to dry-out case, performance effect of flooded condenser can also be implemented.
- Since developed methodology is validated, numerical models can be employed in an optimization tool to optimize thermal performance of a FGHP. Such optimization study can be important from design point of view.

REFERENCES

[1] D. Reay, "The perkins tube—a noteworthy contribution to heat exchanger technology," *Journal of Heat Recovery Systems (2/2)*, pp. 173–187, 1982.

[2] H. Chaudhry, B. Hughes, and S. Ghani, "A review of heat pipe systems for heat recovery and renewable energy applications," *Renewable and Sustainable Energy Reviews*, pp. 2249–2259, 2012.

[3] F.-T. W. Structures, "https://www.frostytech.com/articles/2466/index.html accessed: 04.2021."

[4] X. Chen, H. Ye, X. Fan, T. Ren, and G. Zhang, "A review of small heat pipes for electronics," *Applied Thermal Engineering*, pp. 1–17, 2016.

[5] W. Xing, A. Ullmann, N.Brauner, J. Plawsky, and Y. Peles, "Advancing microscale cooling by utilizing liquid-liquid phase separation," *In: Scientific Reports (8/1)*, pp. 2–11, 2018.

[6] Y. Ling, X. Zhang, F. Wang, and X. She, "Performance study of phase change materials coupled with three-dimensional oscillating heat pipes with different structures for electronic cooling," *In: Renewable Energy (154),*, pp. 636–649, 2020.

[7] H. Zhang, M. Mi, J. Miao, L. Wang, Y. Chen, T. Ding, X. Ning, and Y. Huo, "Development and on-orbit operation of loop heat pipes on chinese circumlunar return and reentry spacecraft," *In: Journal of Mechanical Science and Technology (31/6)*, pp. 2597–2605, 2017.

[8] S. Ghani, S. Gamaledin, M. Rashwan, and M. Atieh, "Experimental investigation of double-pipe heat exchangers in air conditioning applications," *In: Energy and Buildings*, pp. 801–811, 2018.

[9] C.Wang, J. Chen, S. Qiu, W. Tian, D. Zhang, and G. Su, "Performance analysis

of heat pipe radiator unit for space nuclear power reactor," *Annals of Nuclear Energy*, pp. 74–84, 2017.

[10] S. D. Schampheleire, K. D. Kerpel, T. Deruyter, P. D. Jaeger, and M. D. Paepe, "Experimental study of small diameter fibres as wick material for capillary-driven heat pipes," *Applied Thermal Engineering*, pp. 258–267, 2015.

[11] A. Faghri, "Heat pipes: Review, opportunities and challenges," *In: Frontiers in Heat Pipes (5/1)*, 2014.

[12] F. Lefevre, J. Conrardy, M. Raynaud, and J. Bonjour, "Experimental investigations of at plate heat pipes with screen meshes or grooves covered with screen meshes as capillary structure," *Applied Thermal Engineering*, p. 95, 2012.

[13] X. Li, M. Li, M. Li, R. Wu, Y. Wan, and T. Cheng, "Forming method of micro heat pipe with compound structure of sintered wick on grooved substrate," *Heat and Mass Transfer*, pp. 581–593, 2016.

[14] G. Grover, T. Cotter, and G. Erickson, "Structures of very high thermal conductance," *Journal of Applied Physics (35/6)*, pp. 1990–1991, 1964.

[15] T. Cotter, "Principles and prospects for micro heat pipes," 1984.

[16] B. Babin, G. Peterson, and D. Wu, "Steady-state modeling and testing of a micro heat pipe," *Journal of Heat Transfer*, 1990.

[17] D. Khrustalev and A. Faghri, "Thermal analysis of a micro heat pipe," *Journal of Heat Transfer*, pp. 189–198, 1994.

[18] G. Peterson and H. Ma, "Theoretical analysis of the maximum heat transport in triangular grooves: A study of idealized micro heat pipes," *Journal of Heat Transfer*, pp. 731–739, 1996.

[19] J. Qu, H. Wu, and P. Cheng, "Effects of functional surface on performance of a micro heat pipe," *International Communications in Heat and Mass Transfer*, pp. 523–528, 2008.

[20] M. Kumar and S. Dasgupta, "Modelling of evaporation from v-shaped microgrooves," *Chemical Engineer Community*, pp. 225–248, 1997.

[21] B. Suman, S. De, and S. Dasgupta, "A model of the capillary limit of a micro heat pipe and prediction of the dry-out length," *International Journal of Heat and Fluid Flow*, pp. 495–505, 2005.

[22] B. Suman and N. Hoda, "Effect of variations in thermophysical properties and design parameters on the performance of a v-shaped micro grooved heat pipe," *International Journal of Heat and Mass Transfer*, pp. 2090–2101, 2005.

[23] C. Zhang, Y. Chen, M. Shi, and G. Peterson, "Optimization of heat pipe with axial omega-shaped micro grooves based on a niched pareto genetic algorithm (npga)," *Applied Thermal Engineering*, pp. 3340–3345, 2009.

[24] Y. Chen, C. Zhang, M. Shi, J. Wua, and G. Peterson, "Study on flow and heat transfer characteristics of heat pipe with axial omega-shaped micro grooves," *Applied Thermal Engineering*, pp. 3340–3345, 2009.

[25] K. Do, S. Kim, and S. Garimella, "A mathematical model for analyzing the thermal characteristics of a flat micro heat pipe with a grooved wick," *International Journal of Heat and Mass Transfer*, pp. 4637–4650, 2008.

[26] L. Lin, R. Ponnapan, and J. Leland, "High performance miniature heat pipe," *International Journal of Heat and Mass Transfer*, pp. 3131–3142, 2002.

[27] R. Hopkins, A. Faghri, and D. Khrustalev, "Flat miniature heat pipes with micro capillary grooves," *ASME J. Heat Transfer*, pp. 102–109, 1999.

[28] R. Rullière, F. Lefèvre, and M. Lallemand, "Prediction of the maximum heat transfer capability of two-phase heat spreaders – experimental validation," *International Journal of Heat and Mass Transfer*, pp. 1255–1262, 2007.

[29] F. Lefèvre, R. Rullière, G. Pandraud, and M. Lallemand, "Prediction of the temperature field in flat plate heat pipes with micro-grooves – experimental validation," *International Journal of Heat and Mass Transfer*, pp. 4083–4094, 2008.

[30] G. Odabaşı, "Modeling of multidimensional heat transfer in a rectangular grooved heat pipe," *PhD thesis, Middle East Technical University,Ankara,Turkey*, 2014.

[31] F. Lefèvre and M. Lallemand, "Coupled thermal and hydrodynamic models of flat micro heat pipes for the cooling of multiple electronic components," *International Journal of Heat and Mass Transfer*, pp. 1375–1383, 2006.

[32] R. Revellin, R. Rullière, F. Lefèvre, and J. Bonjour, "Experimental validation of an analytical model for predicting the thermal and hydrodynamic capabilities of flat micro heat pipes," *Applied Thermal Engineering*, pp. 1114–1122, 2009.

[33] S. Lips, F. Lefèvre, and J. Bonjour, "Combined effects of the filling ratio and the vapour space thickness on the performance of a flat plate heat pipe," *International Journal of Heat and Mass Transfer*, pp. 694–702, 2010.

[34] S. Lips, F. Lefèvre, and J. Bonjour, "Physical mechanisms involved in grooved flat heat pipes: Experimental and numerical analyses," *International Journal of Heat and Mass Transfer*, pp. 1243–1252, 2011.

[35] M. Aghvami and A. Faghri, "Analysis of flat heat pipes with various heating and cooling configurations," *Applied Thermal Engineering*, pp. 2645–2655, 2011.

[36] U. Vadakkan, S. Garimella, and J. Murthy, "Transport in flat heat pipes at high heat fluxes from multiple discrete sources," *ASME J. Heat Transfer 126*, 2004.

[37] H. Shabgard and A. Faghri, "Performance characteristics of cylindrical heat pipes with multiple heat sources," *Applied Thermal Engineering*, pp. 3410–3419, 2011.

[38] F. Lefèvre, S. Lips, and J. Bonjour, "Investigation of evaporation and condensation processes specific to grooved flat heat pipes," *Frontiers in Heat Pipes*, 2010.

[39] R. Sonan, S. Harmand, J. Pellé, D. Leger, and M. Fakès, "Transient thermal and hydrodynamic model of flat heat pipe for the cooling of electronics components," *International Journal of Heat and Mass Transfer*, pp. 6006–6017, 2008.

[40] S. Harmand, R. Sonan, M. Fakès, and H. Hassan, "Transient cooling of electronic components by flat heat pipes," *Applied Thermal Engineering*, pp. 1877–1885, 2011.

[41] V. Guichet, N. Khordehgah, and H. Jouhara, "Experimental investigation and analytical prediction of a multi-channel flat heat pipe thermal performance," *International Journal of Thermofluids*, 2020.

[42] P. C. Stephan and C. A. Busse, "Analysis of the heat transfer coefficient of grooved heat pipe evaporator walls," *International Journal of Heat and Mass Transfer*, p. 383, 1992.

[43] Y. Zhang and A. Faghri, "Numerical simulation of condensation on a capillary grooved structure," *Numerical Heat Transfer, Part A*, pp. 227–243, 2001.

[44] G. Gökçe, "Development of a cfd assisted 3-d modeling and analysis methodology for grooved heat pipe design and performance assessment," *PhD Thesis, Middle East Technical University,Ankara,Turkey*, 2020.

[45] S. Saygan, "Modeling guided heat pipe design methodology and experimental validation for flat grooved heat pipes," *PhD Thesis, Middle East Technical University,Ankara,Turkey*, 2021.

[46] M. Potash and P. Wayner, "Evaporation from a two-dimensional extended meniscus," *International Journal of Heat and Mass Transfer*, pp. 1851–1863, 1972.